3D printing of Continuous Fiber Reinforced Composites: A Review of the Processing, Pre- and Post-Processing Effects on Mechanical Properties

Faraz Safari, Abdolvahed Kami*, Vahid Abedini

Faculty of Mechanical Engineering, Semnan University, Semnan, Iran

*Corresponding Author's Email: akami@semnan.ac.ir

Abstract

The main objective of this study is to review existing research on the application of fused deposition modeling (FDM) for 3D printing of continuous fiber reinforced composites (CFRCs). An overview of additive manufacturing (AM) technology production techniques are provided first, followed by a look into FDM technology. The articles on CFRC printing were then summarized. The type of reinforcing material and matrix utilized, the research subject, the mechanical properties investigated, and the sample dimensions are all listed. Various pre-processing, processing, and post-processing conditions, as well as their impact on CFRC mechanical properties, were also discussed.

Keywords:

Additive manufacturing, 3D printing, Continuous fiber reinforced composites, Carbon fiber, Fused filament fabrication, Fused deposition modeling

1. Abbreviations

Table 1. List of abbreviations

AM	Additive Manufacturing
3DP	Three-Dimensional Printing
ABS	Acrylonitrile Butadiene Styrene
BIS	Beam Interference Solidification
BPM	Ballistic Particle Manufacturing
CF	Carbon Fiber
CFRC	Continuous Fiber Reinforced Composites
DMD	Direct Metal Deposition
DMLS	Direct Metal Laser Sintering
EBM	Electron Beam Melting
FDM	Fused Deposition Modeling
FFF	Fused Filament Fabrication
FVF	Fiber Volume Fraction
GF	Glass Fiber
HIS	Holographic Interference Solidification
IJP	Inkjet Printing
KF	Kevlar Fiber
LENS	Laser Engineered Net Shaping
LOM	Laminated Object Manufacturing
LPD	Laser Powder Deposition
LTP	Liquid Thermal Polymerization

MJM	Multijet Modeling
PLA	Polylactic Acid
POM	Polyoxymethylene
SFP	Solid Foil Polymerization
SGC	Solid Ground Curing
SLA	Stereo Lithography
SLC	Selective Laser Cladding
SLM	Selective Laser Melting
SLS	Selective Laser Sintering
TPU	Thermoplastic Polyurethane

2. Introduction

As depicted in Fig. 1, formative manufacturing (injection molding, casting, stamping, and forging), subtractive manufacturing (milling, drilling, and turning), and additive manufacturing are the three types of manufacturing processes. The first two are traditional manufacturing technologies that have offered fewer attractions in recent decades when compared to additive manufacturing (AM) technology [1].

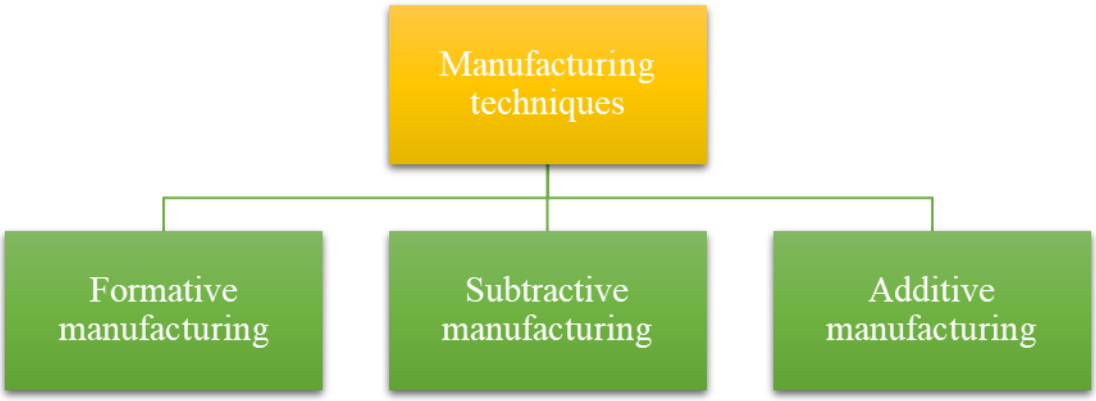

Fig. 1 Classification of manufacturing techniques

The layer-by-layer creation of an item from 3D model data utilizing multiple raw materials is referred to as AM technology, often known as 3D printing. In recent years, it has made significant development and is now regarded as a creative solution to many of the difficulties that traditional manufacturing methods confront. Its use is continuously developing, and the technology is improving regularly. AM decreases build time and cost, enhances operational flexibility, allows for quick prototyping, minimizes supply chain load, and, most significantly, can manufacture nearly anything that can be designed in CAD software. It's simple to predict that AM will be the obvious answer for designers and manufacturers all around the world in less than a decade. Aerospace [2, 3], automotive [3], manufacturing, treatment [4-6], research, architecture [7, 8], art [9], food [10-12], and apparel [13-15] are some of the applications of AM technology.

As illustrated in Fig. 2, AM processes are split into various categories. Powder, liquid, and solid (filament) are the basic materials utilized in 3D printers (as seen at the bottom of Fig. 2, with green for powder, blue for liquid, and red for solid).

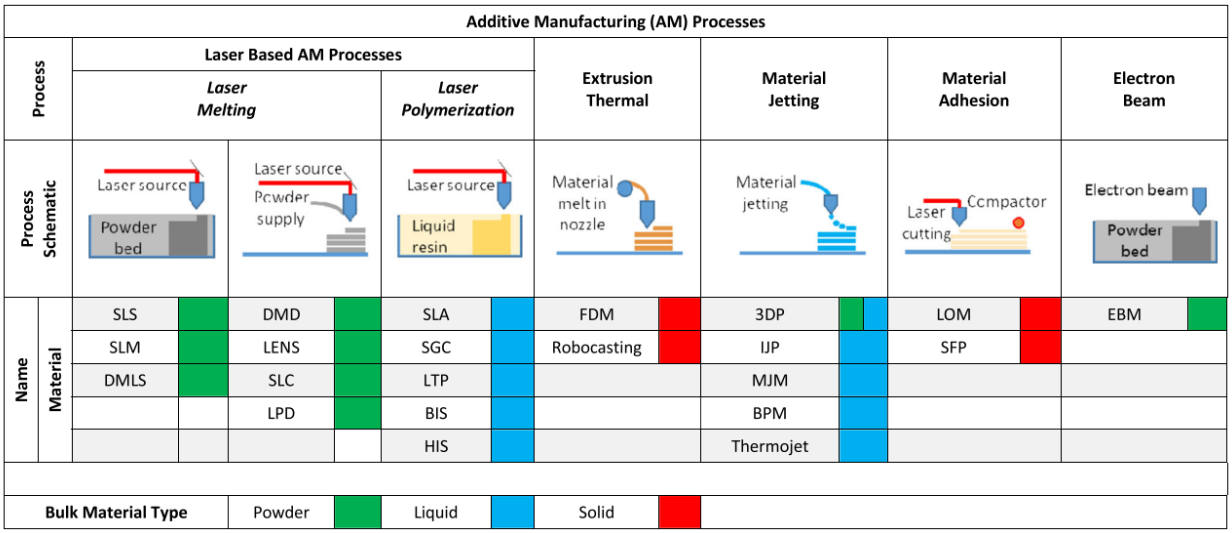

Fig. 2 Different categories of AM processes [16]

Laser melting methods include Selective Laser Sintering (SLS), Selective Laser Melting (SLM), Direct Metal Laser Sintering (DMLS), Electron Beam Melting (EBM), Laser Engineered Net Shaping (LENS), Direct Metal Deposition (DMD), Laser Powder Deposition (LPD), and Selective Laser Cladding (SLC). A laser source is used to selectively melt a material provided in the form of fine powder in laser melting AM techniques. After that, the material cools and solidifies to produce the final component. The laser beam is being guided in the x-y plane by scanning optics, while a table travels in the z-direction. Laser polymerization, which includes prototyping technologies like Stereo Lithography (SLA), Solid Ground Curing (SGC), Liquid Thermal Polymerization (LTP), Beam Interference Solidification (BIS), and Holographic Interference Solidification (HIS), employs a liquid photosensitive resin that solidifies when illuminated by a (usually low-power) laser source. This disposable plastic material is used to create fine-cut pieces with a smooth surface for jewelry, dentistry, and medical applications. Extrusion processes include technologies such as Fused Deposition Modeling (FDM), Robocasting, and material extrusion

techniques that employ a heated extrusion nozzle to soften or melt material, generally plastic, in the form of wire. After being melted, the material is extruded via an extrusion nozzle, which deposits the material before cooling to solidify and produce the final component shape. Material jetting technologies include Three-Dimensional Printing (3DP), Inkjet Printing (IJP), Multijet Modeling (MJM), Ballistic particle manufacturing (BPM), and Thermojet. Material jetting processes use multiple thin nozzles to "spray" either molten material or, more commonly, a binder (adhesive) to bind the powder in a solid object. The working concept of the process is similar to that of all laser-melting procedures, except that no phase transition occurs; instead, the binder binds the powder particles together. Adhesive-based processes include technologies such as Laminated Object Manufacturing (LOM), Solid Foil Polymerization (SFP), and others. However, adhesive-based processes are no longer widely used. The working concept comprises a cutter (often a laser) that cuts a thin coating of paper or plastic in the required outlines. The film is then pushed down over the preceding one by a heated compactor, activating a heat-curing adhesive located on the film's downward face, allowing it to be attached to the substrate. Electron beam procedures are similar to laser-melting processes, except that an electron beam is utilized as an energy source instead of a laser beam to melt or sinter the material.

A review of prior research on the manufacturing of continuous fiber reinforced composites (CFRCs) with FDM technology is provided in this publication. The influence of various pre-processing, processing (printing), and post-processing conditions on the mechanical properties of CFRCs has been investigated.

3. Fused Deposition Modeling

FDM technology, also known as FFF, is one of the most important AM methods that is based on solids and has become more desirable and attractive to industries and, most importantly, to the

general public due to its simplicity, flexibility, fast prototyping, low cost, minimal waste, and ease of material change [17, 18]. Because of their temperature characteristics, thermoplastic base filaments are the most commonly utilized in FDM. This technique may create components from thermoplastic filaments like PLA, ABS, Nylon, polypropylene (PP), polyether-ether-ketone (PEEK), and polyamides (PA) like PA6, PA12 [19-21]. This technique is a well-known technology that Crump [22] patented in 1989.

FDM 3D printing involves the deposit of a thermoplastic filament. A piece of filament from a reel is extruded in the XY plane, forming a layer of solid material on the build plate, after passing through a hot head at a temperature greater than the melting point of the filament. A model may be created by laying a layer shape and then filling the interior with plasticized material using a zigzag motion of the head. After printing one layer, the head travels along the Z-axis, causing the next layer to be built up. Using this approach, complicated forms with minimal preparation could be constructed [23]. The required item is developed in one CAD software, converted to an STL file, and then delivered to the machine for printing.

Using reinforcing fibers enhances strength and hardness, and these reinforcing fibers have excellent properties including high strength, lightweight, and anti-corrosion. As illustrated in Fig. 3, there are two forms of fiber-reinforced printing: short and continuous. The mechanical characteristics of CFRC (such as Young's modulus, tensile strength, and flexural strength) are significantly higher than those of short fiber reinforced or plain components (see Fig. 4).

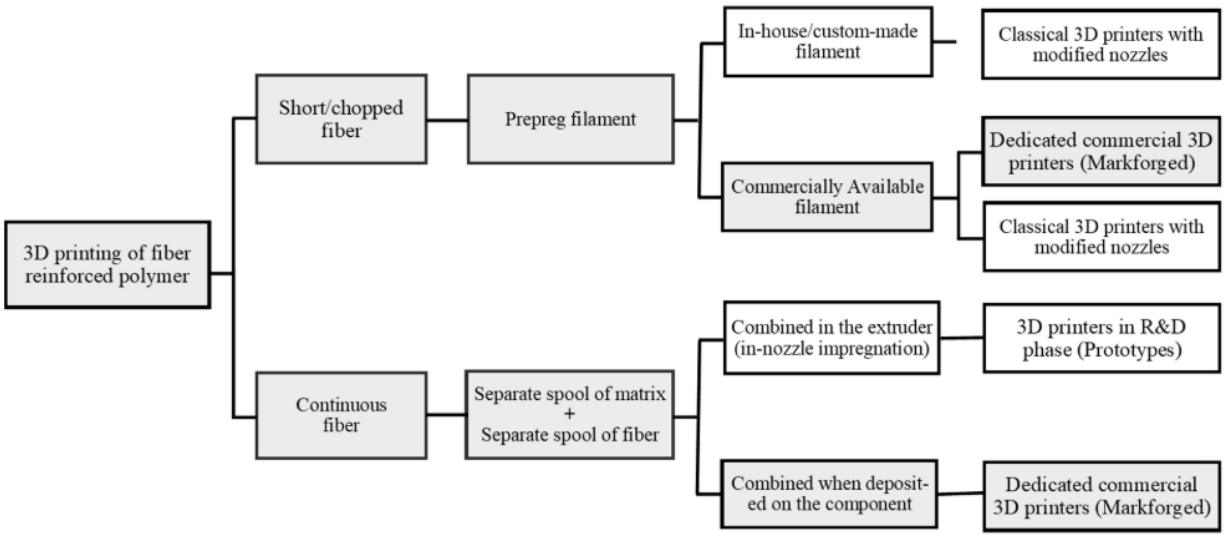

Fig. 3 3D-printed fiber-reinforced polymer manufacturing process classification [24]

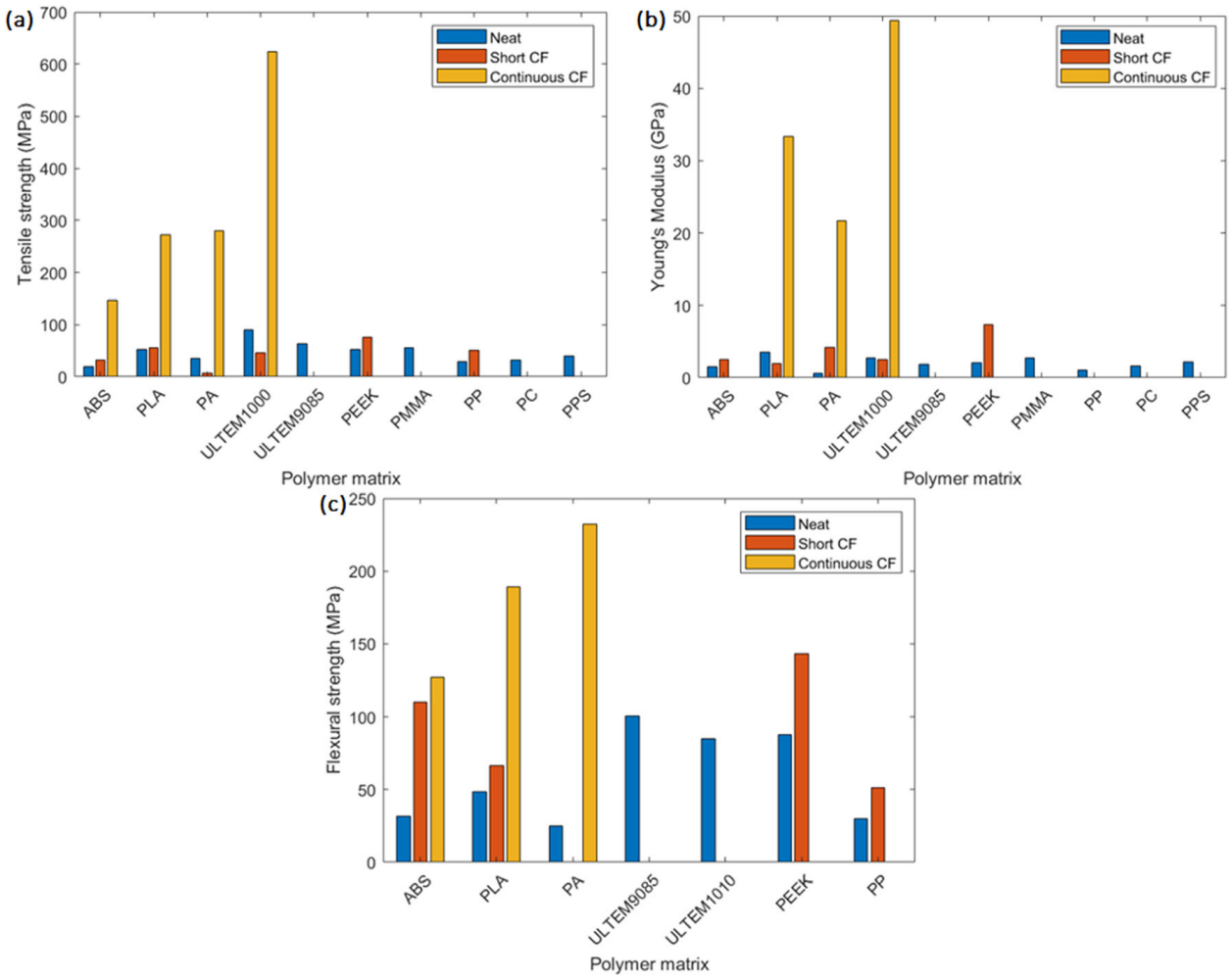

Fig. 4. Overall mechanical performance for FFF-produced specimens. Average (a) tensile strength, (b) Young's modulus, and (c) flexural strength values for neat, short CF reinforced, and continuous CF reinforced specimens [25]

4. Mechanisms of Fiber-reinforced material's 3D printers

Co-extrusion, dual extrusion, multi-degree of freedom, and compaction roller methods are four popular approaches for 3D printing CFRC [25-27]. Fig. 5 illustrates the schematics of these approaches. In the co-extrusion technique, the thermoplastic string and the reinforcing fiber are added separately to the head of the printing machine. In the dual extrusion method, the

thermoplastic filament and the fiber-reinforced are extruded separately through two nozzles on the build platform [25]. The multi-degree of freedom method uses a robotic arm system to produce fiber-reinforced and thermoplastic [26]. In the compaction roller technique, a cartridge heater was secured to the nozzle body and used as a fixed shaft to support the compaction roller. The compaction roller had internal bearings to allow it to rotate freely around the cartridge heater.

The thermoplastic string and reinforcing fiber are introduced independently to the printing machine's head in the co-extrusion technique. The thermoplastic filament and the fiber-reinforced filament are extruded separately through two nozzles on the construction platform in the dual extrusion technique [25]. The multi-degree of freedom technique [26] makes fiber-reinforced and thermoplastic materials with a robotic arm system. In the compaction roller technique, a cartridge heater was attached to the nozzle body and utilized as a fixed shaft to support the compaction roller. Internal bearings allowed the compaction roller to freely spin around the cartridge heater. The compaction roller itself was heated by the cartridge heater [27].

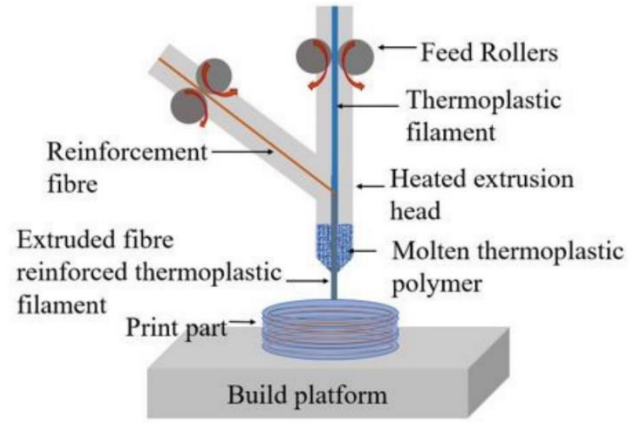

(a)

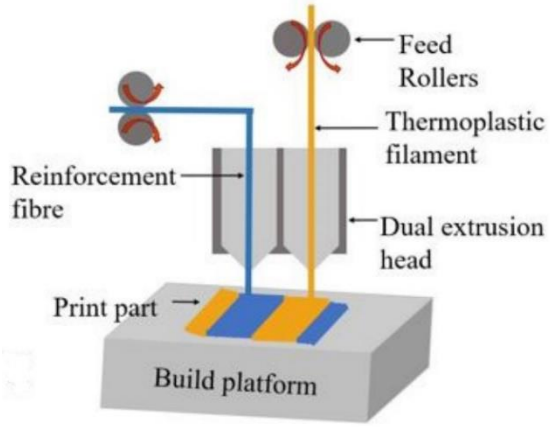

(b)

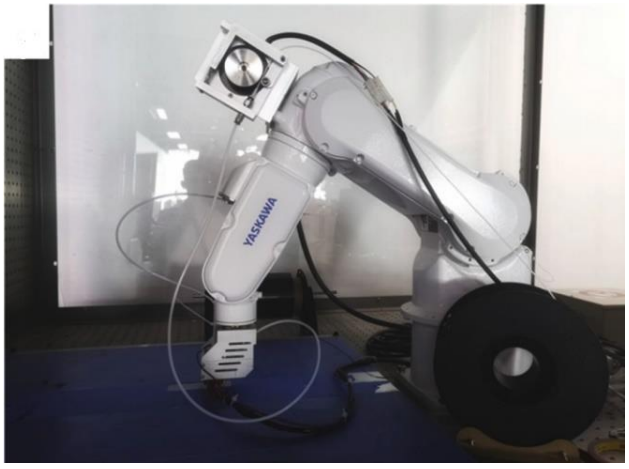

(c)

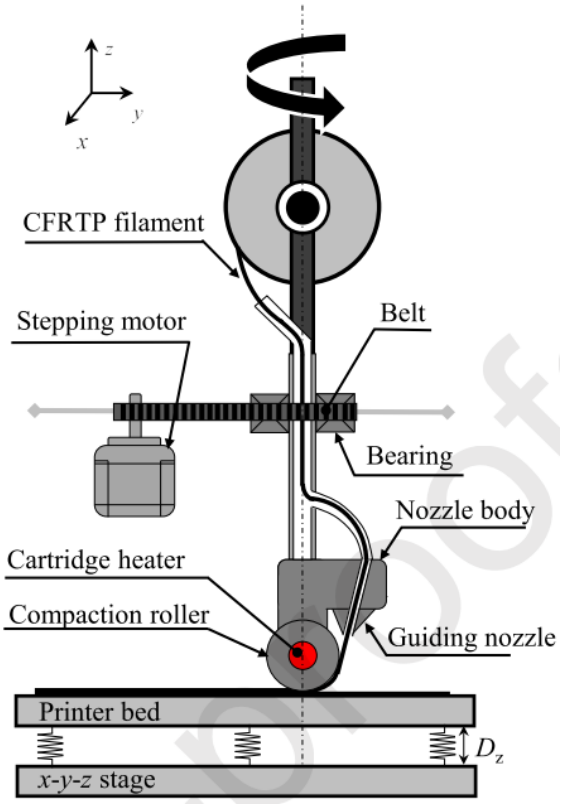

(d)

Fig. 5 Schematic illustration of the various mechanisms of 3D printers for printing fiber-reinforced samples with (a) co-extrusion FDM printer [25], (b) dual-extrusion FDM printer [25], (c) multi-degree of freedom [26], and (d) compaction roller [27].

5. An overview of CFRC 3D printing research

In this article, the authors attempted to review all papers related to CFRC 3D printing. Table 2 summarizes these works and includes a list of the authors, publication year, study topic, matrix material, fiber-reinforced material, printer utilized, mechanical characteristics evaluated, and sample standards for those publications. Furthermore, a summary of 3D printed CFRC's mechanical properties along with their processing (printing), pre-/post-processing conditions are presented in Table 3. In comparison to CFRCs manufactured conventionally, printed CFRCs have inferior mechanical characteristics. The existence of flaws such as vacancies and poorer layer bonding are two primary reasons for this. As a result, several studies have attempted to enhance the mechanical characteristics of CFRCs by various methods such as impregnation, rolling, pressing, and heat treatment (see Fig. 11). In addition,

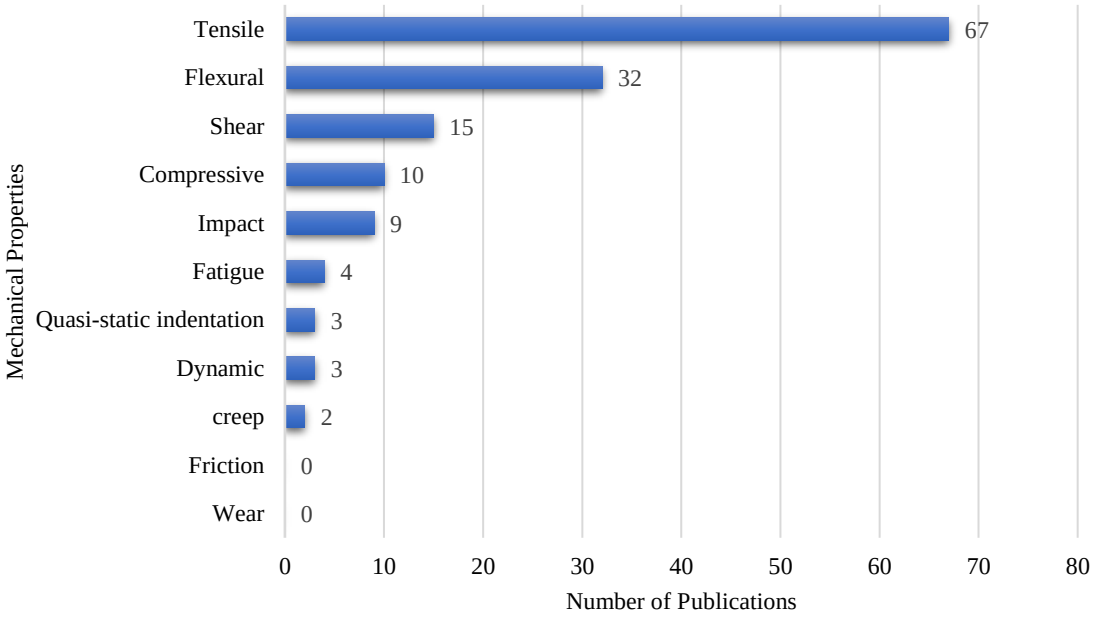

Fig. *6* shows the number of papers on mechanical properties, with tensile and flexural testing being the most popular among academics. As a result, just the tensile and flexural properties of the 3D printed CFRCs will be discussed. Another thing to note is that no papers have focused on the wear

and friction experiments (as depicted in

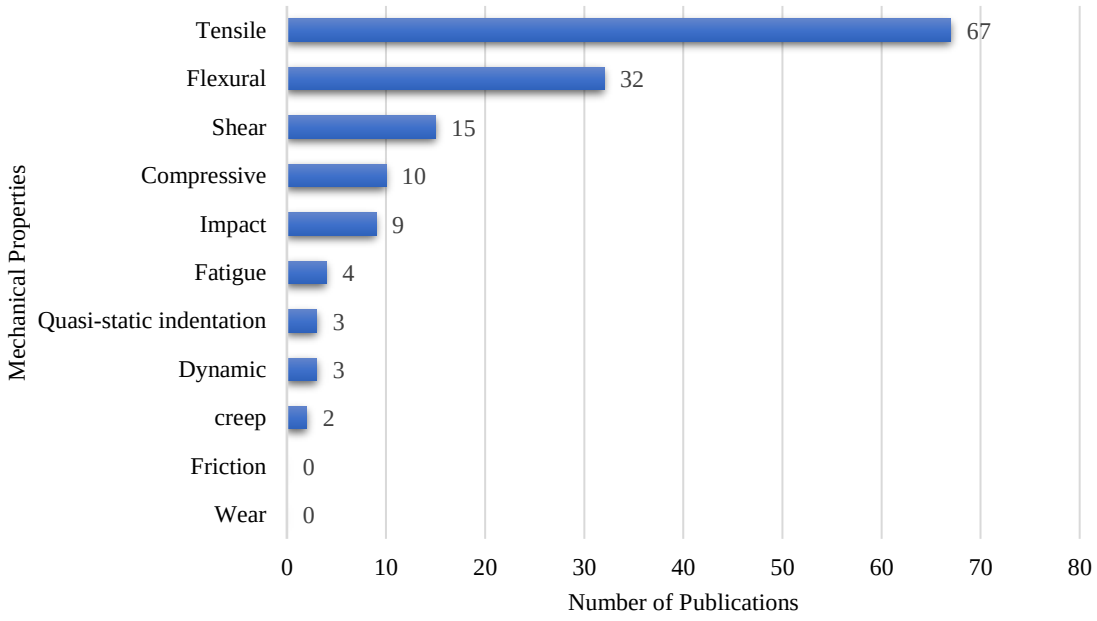

Fig. *6*), which could be interesting subjects for future researches. In addition,

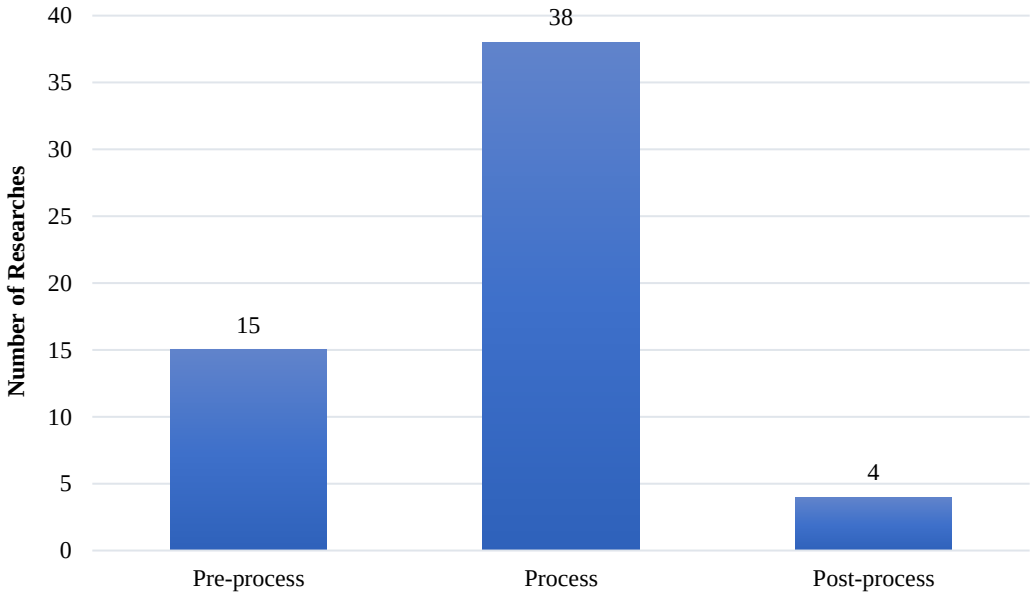

Fig. *7* divides CFRC research into three categories: pre-processing, processing, and post-processing. As can be seen, the majority of the study focuses on the processing conditions, with

just a few studies focusing on improving the mechanical characteristics of CFRC through postprocessing. As a result, it might be an intriguing topic for future research.

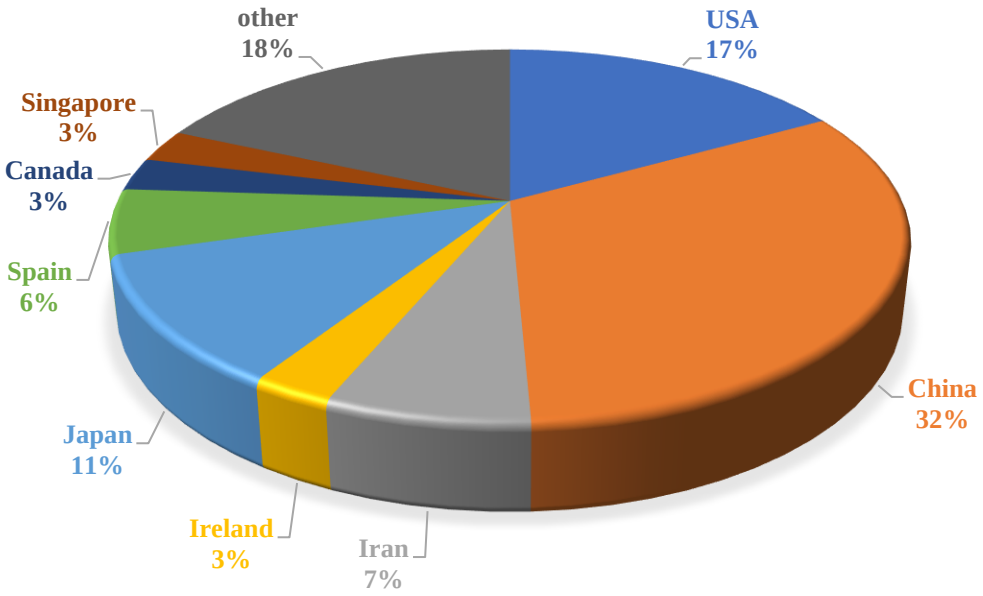

Fig. *8* shows a list of the nations where the studies were done. China, the United States, Japan, Iran, Spain, Ireland, Canada, and Singapore are the nations that have concentrated on CFRC 3D printing, according to this graph. Many businesses have succeeded in developing and manufacturing 3D printers, particularly FDM. Different varieties of these printers have been used to produce examples in the literature, however many publications have used Markforged's

MarkOne and MarkTwo 3D printers (see

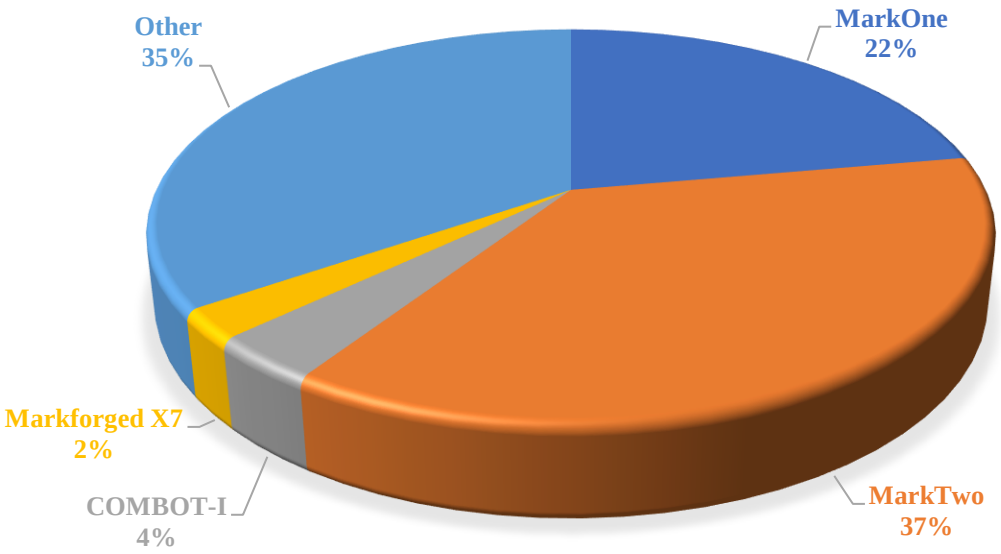

Fig. 9).

The number of publications published on the subject of CFRC 3D printing has been growing every year, as shown in

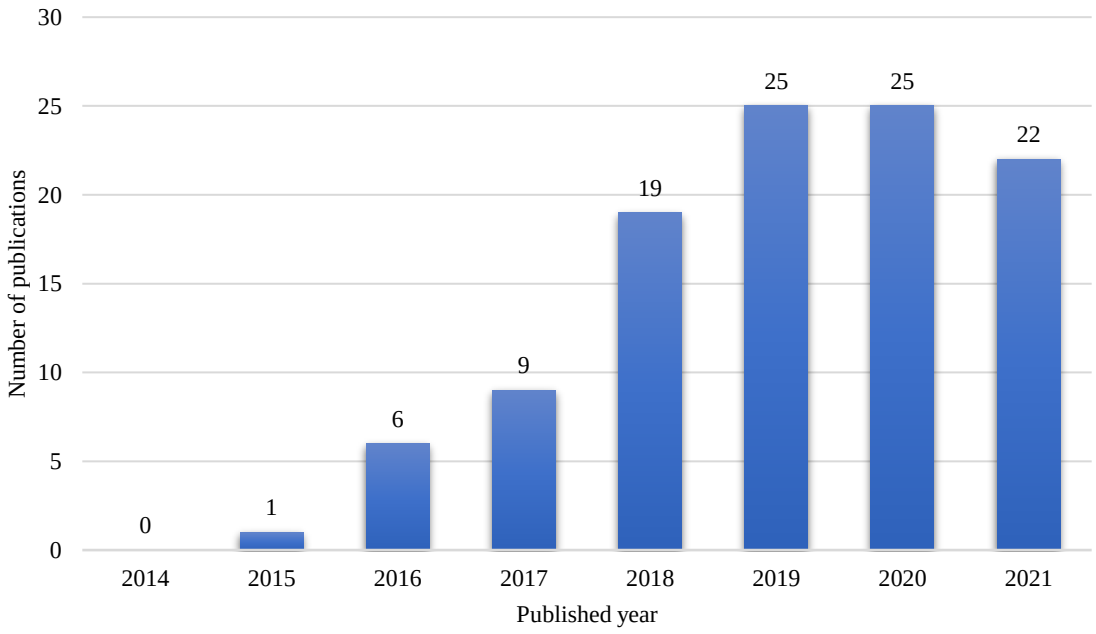

Fig. *10*. In contrast to the trend, there was no rise in the number of papers published in 2020. This might be related to the coronavirus epidemic and most nations' quarantine policies. Given that this article is being written in the middle of 2021, a substantial number of articles have already been published in 2021, implying that by the end of 2021, the number of articles published will be significantly greater than in 2020.

Table 2. A summary of CFRC 3D printing research studies

Author/Authors	Published Year	Research Object	Matrix Material	Reinforcement Material	3D Printer	Studied Mech. Prop.	Specimen Design
Akhoundi et al. [28]	2020	In-melt simultaneous impregnation	PLA, PLA+, PLA-wood, TPU, HDglass, POM, PA+CF	GF	-	Tensile	ASTM D638, type IV
Akhoundi et al. [17]	2019	Improving mechanical properties	PLA	GF	-	Tensile, bulk density	ASTM D638, type IV, ASTM D792
Al Abadi et al. [18]	2018	Evaluation of elastic properties	Nylon	CF, GF, KF	MarkOne	Tensile	ASTM D3039
Araya-Calvo et al. [29]	2018	Improving mechanical properties	Onyx	CF	MarkTwo	Compressive, Flexural	ASTM D695, ASTM D790
Babu et al. [30]	2021	Influence of slicing parameters on surface quality and mechanical properties	PLA	CF	Raise 3D V2 N2	Tensile, Flexural, Interlaminar shear strength	ASTM D638, ASTM D790, ASTM D2344
Baumann et al. [31]	2017	Investigation of a new approach for additively manufactured continuous fiber-reinforced polymers	ABS	CF, GF	-	Tensile	ISO 527
Bettini et al. [32]	2017	Improving mechanical properties	PLA	Aramid	Blue Tek Strato	Tensile, Compressive	for tensile tests 250 mmx15 mmx0.95 mm/for compression tests 60 mmx21.3 mmx1.5 mm
Caminero et al. [33]	2018	Improving Impact damage resistance	Nylon	CF, GF, KF	MarkTwo	Impact	ASTM D6110
Cersoli et al. [34]	2021	Evaluation mechanical properties	PLA	KF	MakerGear M2	Tensile, Flexural,	ASTM D3039, ASTM D7264, 100 x 100 x 5.5

						Impact	
Chacon et al. [35]	2019	Effect of process parameters on mechanical properties	Nylon	CF, GF, KF	MarkTwo	Tensile, Flexural	ASTM D3039, ASTM D790
Chaudhry et al. [36]	2019	Effect of CF on reinforcement of thermoplastics using FDM and RSM	PLA	CF	ANET A-8M	Tensile, Flexural	ASTM-D3039/D3039M, ASTM-D638, ASTM-D790, ASTM-D7264/D7264M
Chen et al. [37]	2021	Optimization of printing parameters	PLA	GF	-	Tensile, Flexural, Impact, Short beam shear	GB/T1447-2005, GB/T 1449-2005, GB/T 1451-2005, JC/T 773-2010
Chen et al. [38]	2021	Evaluation of mechanical properties & fracture behavior	Onyx	CF	MarkTwo	Tensile	ASTM D638-14 Type IV
Dickson et al. [39]	2017	Influence of process parameters on mechanical properties	Nylon	CF, GF, KF	MarkOne	Tensile, Flexural	ASTM D3039, ASTM D790
Dikshit et al. [40]	2019	Quasi-static indentation analysis	CR-WT	KF	MarkOne, InkJet	Quasi-static indentation	ASTM D6264
Dong et al. [41]	2018	Evaluating mechanical properties	Nylon	KF	MarkOne	Tensile	ASTM D3039
Dong et al. [42]	2021	Mechanical properties and shape memory effect of 4D printed cellular structure composite	PLA	KF	Createbot MID250	Tensile	ASTM D3039
Dong et al. [43]	2020	Diamond cellular structural	PLA	KF	Createbot MID250	Tensile	ASTM D3039
Dugbenoo et al. [44]	2018	Enhanced bonding	Nylon	CF, GF, KF	MarkOne	single-lap-joint (SLJ)	ASTM D2093

Dutra et al. [45]	2019	Mechanical characterization and asymptotic homogenization	Nylon	CF	MarkOne	Tensile, Compression, In-plane shear	ASTM D3039, ASTM D638, ASTM D6641, ASTM D3518
Fernandes et al. [46]	2021	Evaluation mechanical properties	Onyx	CF	MarkTwo	Tensile, Interlaminar shear, Dynamic mechanical analysis	ASTM D638 -14, ASTM D3039/D3039M-17, ASTM-D2344/D2344M, ASTM D4056 -12
Ghebretinsae et al. [47]	2019	Strength analysis with using experimental and numerical methods	Onyx	CF	MarkTwo	Tensile, Flexural	ASTM D3039, ASTM D7264
Giannakis et al. [48]	2019	Static and fatigue properties	Nylon, PLA	CF	BCN3D, MarkTwo	Tensile, Fatigue	ASTM D3039, custom specimens
Goh et al. [49]	2018	Characterization of mechanical properties and fracture mode	Nylon	CF	MarkOne	Tensile, Flexural, Quasi-static indentation	ASTM D3039, ASTM D790, ASTM D6264
Gonzalez-Estrada et al. [50]	2018	Evaluation mechanical properties	Nylon	CF, GF	MarkTwo	Tensile	ASTM D638, type IV
Hao et al. [51]	2018	Preparation and characterization	Epoxy resin	CF	-	Tensile, Flexural	ISO 527, ISO 178
Hedayati et al. [52]	2020	Study on mechanical and cell viability properties	PCL	PGA suture	-	Tensile	ASTM D638, ASTM D2256
Heidari-Rarani et al. [53]	2019	Improving mechanical properties	PLA	CF	-	Tensile, Flexural	ASTM D638, ASTM D3039, ASTM D790
Hetrick et al. [54]	2021	Charpy impact energy absorption	Onyx	KF	MarkTwo	Charpy impact	ASTM D6110

Hou et al. [55]	2020	A constitutive model for 3d printed CFRC structures with variable fiber content	PLA	KF	COMBOT-I	Tensile, Compressive, In-plane shear	GB/T 3354-2014, GB/T 1448-2005, GB/T 3355-2014
Hu et al. [56]	2018	Manufacturing and 3D printing of prepreg filament	PLA	CF	Mendel	Flexural	60 mm x11 mm x3layer thickness
Hu et al. [57]	2021	Fiber damage during 3D printing	-	CF-PLA	MarkTwo	Tensile, Compressive	200mm x 150mm x 2mm, 12mm x 12mm x 30mm
Ibrahim et al. [58]	2020	Thermal conductivity	Nylon	CF	MarkOne	Effective thermal conductivity	Variable
Imeri et al. [59]	2018	Fatigue analysis	Nylon	CF, GF, KF	MarkTwo	Fatigue	ASTM E606M
Ipekci et al. [60]	2021	Experimental and statistical analysis of robotic 3D printing	photopolymer	GF	NACHI brand MZ07L	Tensile, Flexural, izod impact	ASTM D3039, ASTM D7264, ASTM D256
Iraqi et al. [61]	2019	Evaluate the mechanical properties	Onyx	CF	MarkTwo	Tensile, In-plane shear, Interlaminar shear resistance	ASTM D3039, ASTM D518, ASTM D2344
Ishii et al. [62]	2018	Bending fracture rule	Nylon	CF	MarkTwo	Bending fracture	Curved CF
Jahangir et al. [63]	2019	Porosity reduction	Polycarbonate (PC)	CF	400mc	Tensile, Warp	ASTM D638
Justo et al. [64]	2018	Mechanical characterization of long fiber composites	Nylon	CF, GF	MarkOne	Tensile, Compressive, In-plane shear	ASTM D3039, ASTM D695-02a, ASTM D3518

Kabir et al. [65]	2020	Impact resistance and failure mechanism of cellular composites	Nylon white	GF	MarkTwo	Drop-weight impact, Charpy and Izod impact	ASTM D3763, ASTM D6110
Kousiatza et al. [66]	2019	A methodological study using fiber Bragg grating sensors	Nylon	CF, GF	MarkTwo	residual strains, Thermal strains	40 mm length x 20 mm width, while 10.125 mm (81 layers) and 10.100 mm (101 layers) were the thicknesses of the carbon and the glass fiber reinforced composite
Li et al. [67]	2019	The quantitative analysis of mechanical properties	PLA	CF	-	tensile strength	240mm x 12.5mm x 2mm
Li et al. [68]	2016	Rapid prototyping	PLA	CF	-	Tensile, Flexural, Dynamic mechanical analyzer	110 mm long 27 mm width and 2.3 mm thick, 55 mm long 12 mm width and 2.3 mm thick, 35 mm long 12 mm width and 2.3 mm thick
Liu et al. [69]	2018	Evaluate the mechanical properties	PA6, Carbon nanotube (CNT), graphene nano platelet (GNP)	KF	MarkOne	Tensile	ASTM D638
Liu et al. [70]	2018	Interfacial performance and fracture patterns	PLA	CF	-	Compression	All compression samples had 3 × 3unit cells with a side length of 60 mm, and the thickness of the face sheet was 1.8 mm.

Liu et al. [71]	2018	Free-hanging 3D printing method for lattice truss core structures	PA6	sized CF, virgin CF	COMBOT-I	Flexural, Interlaminar shear	GB/T 1449:2005, JC/T773- 2010 (ISO14130:1997)
Luan et al. [72]	2019	Large-scale deformation and damage detection	PLA	CF	-	Deformation	100mm×100mm×4mm
Luo et al. [73]	2019	Selectively enhanced 3D printing process and performance analysis	PLA	CF	-	Tensile	-
Matsuzaki et al. [74]	2016	In-nozzle impregnation	PLA	CF, Jute Fiber (JF)	Blade-1	Tensile	JIS K 7162
Mei et al. [75]	2019	Filled structures into composites	Nylon	CF, GF, KF	MarkTwo	Tensile	100mm× 10mm× 4mm
Melenka et al. [76]	2016	Evaluation and prediction of the mechanical properties	Nylon	KF	MarkOne	Tensile	ASTM D638-14
Ming et al. [77]	2020	Ultraviolet irradiation	Epoxy	GF	-	Tensile, Three-point Bending, Interlaminar shear	ISO 527, ISO 14125, ISO 14130
Ming et al. [78]	2020	Investigation on process parameters	Epoxy	CF	-	Three-point bending	ASTM D7264
Mohammadizadeh et al. [79]	2018	Creep behavior analysis	Nylon	CF, GF, KF	MarkTwo	Creep, Dynamic thermal analysis	ASTM D-2990-17
Mohammadizadeh et al. [80]	2019	Structural analysis	Nylon	CF, GF, KF	MarkTwo	Tensile, Fatigue, Creep	ASTM D638-14 type I, ASTM E606M, ATSM D2990-17
Mori et al. [81]	2014	Dieless forming	ABS	CF	-	Tensile, Fatigue	-

Mosleh et al. [82]	2021	Determining process-window	ABS	CF	Sizan Lite	Tensile, Flexural, interlaminar shear	ASTM D3039, ASTM D790, ASTM D2344
Nabipour et al. [83]	202۰	Process parameters	ABS	Cu powder	Quantum	tensile strength	ASTM-D638 Type IV
Naranjo-Lozada et al. [84]	2019	Mechanical properties and failure behavior	Nylon	CF	MarkTwo	Tensile	ASTM D638
O'Connor et al. [85]	2019	Low-pressure AM	Nylon	CF, GF, KF	MarkOne	Interlaminar shear	ASTM D2344
Oztan et al. [86]	2019	Microstructure and mechanical properties	PLA, Nylon	CF, KF	MarkOne, Ultimaker 2	Tensile	ASTM D638, ASTM D3039
Peng et al. [87]	2020	Tailorable rigidity and energy-absorption capability	PLA	CF	Mark X	Flexural	90 mm x 6mm x 6mm
Prajapati et al. [88]	2021	Evaluating mechanical, thermal, flame-retardant properties	Onyx	GF, high strength high temperature (HSHT) GF	MarkTwo	Tensile, Impact	ASTM D638, ASTM D256
Prajapati et al. [89]	2021	Effect of fiber volume fraction on the impact strength	Onyx	GF	MarkTwo	Impact strength	ASTM D256
Prajapati et al. [90]	2021	Open hole tensile strength	Onyx	HSHT GF	MarkTwo	Tensile	ASTM D5766
Pyl et al. [91]	2018	Design of test specimens	Nylon	CF	MarkTwo	Tensile, In-plane shear	ASTM D638-14 Type I, ASTM D638 type IV, ASTM D638 type IV modified, ASTM D3039
Qiao et al. [92]	2019	Ultrasonic modification	PLA	CF	MarkOne	Tensile, Flexural	ASTM D3039-14, ASTM D7264-07
Quan et al. [93]	2020	Auxetic honeycomb structures	PLA	KF	-	Tensile, Compression	-

Sanei et al. [94]	2020	Effects of stress concentration on the mechanical properties	Onyx	CF	MarkTwo	Tensile	ASTM D3039
Sanei et al. [95]	2019	Evaluating mechanical properties	Onyx	CF	Markedforged X7	Tensile	ASTM D3039
Sarvestani et al. [96]	2017	Evaluating mechanical properties	Nylon	CF	MarkTwo	Tensile	ASTM D638-14 Type I, ASTM D638-14 Type IV, ASTM D3039
Shang et al. [26]	2020	Inter-line bonding	PLA	CF	Fibertech	Tensile	GB/T3354–2014
Shi et al. [97]	2021	Evaluating mechanical properties	Nylon	KF	MarkTwo	Tensile	ASTM D3039
Shiratori et al. [98]	2021	Evaluating the strength of curved sections of 3D printed specimens	Nylon	CF	MarkTwo	Tensile, Compressive, Three-point bending	ASTM D 6415, L-shape specimen, Flat specimens
Sugiyama et al. [99]	2020	Optimized composites	Nylon	CF	BS01+	Laminate Bearing	ASTM D5961
Sugiyama et al. [100]	2018	Sandwich structures	-	CF	BS01+	Tensile, Three-point bending	JIS K 7165: 2008, JIS K 7017: 1999
Tian et al. [101]	2017	Recycling and remanufacturing	PLA	CF	-	Tensile, Flexural, Interlaminar shear, Impact	GB/T 1447:2005, GB/T 1449:2005, JC/T773- 2010 (ISO14130:1997), GB/T 1043:1993
Tian et al. [102]	2016	Interface and performance	PLA	CF	-	Flexural	ISO 14125:1998
Todoroki et al. [103]	2020	Evaluating mechanical properties	Nylon	CF	MarkTwo	Tensile	Custom specimens with no surface layers

Touchard et al. [104]	2021	Interfacial adhesion quality	PA6	CF	MarkTwo	Tensile, Interlaminar shear	-
Ueda et al. [27]	2020	3D compaction printing	Nylon	CF	MarkTwo	Tensile, Three-point bending	ISO 527-5, ISO 14125
Van der klift et al. [105]	2016	Evaluating mechanical properties	Nylon	CF	MarkOne	Tensile	JIS K 7073
Vaneker et al. [106]	2017	Material extrusion of continuous fiber reinforced plastics using commingled yarn	polypropylene (PP)	GF	MarkOne	Flexural modulus	ISO14125
Wang et al. [107]	2021	Simultaneous reinforcement of both rigidity and energy absorption	Onyx	CF, KF	Mark7	quasi-static indentation	50.0 mm × 50.0 mm × 1.0 mm
Wang et al. [108]	2020	Evaluating Mechanical Properties and microstructures	Pb50Sn50	Cu-CF	COMBOT-I	Tensile	ASTM D3552-96
Wang et al. [109]	2021	Process parameters and mechanical properties	PLA	GF	-	Tensile, Flexural	ISO 14125: 1998
Yang et al. [110]	2017	Mechanism and performance	ABS	CF	-	Tensile, Three-point bending, Interlaminar shear test	ISO 527:1997, ISO 14125:1998, ISO 14130:1998
Yao et al. [111]	2017	Evaluating mechanical properties	PLA	CF	Kossel Rostock Delta D-force	Tensile, Three-point bending	ISO 527-4:1997, ISO 14125: 1998
Yin et al. [112]	2019	Evaluating mechanical properties	PLA	CF	COMBOT-I	Tensile, Flexural, Shielding Effectiveness	The diameters of the brim and crown of the shell were 130 and 100 mm, respectively. The total height was 15 mm

Yu et al. [113]	2019	Mechanical properties behaviors	Onyx	CF	MarkOne	Tensile, Flexural	92.5mm in length and 3.25mm in height, ASTM D6272-17
Zeng et al. [114]	2021	Bending performance and failure behavior of with shape memory capability	PLA	CF	-	Three-point bending	ASTM D7249/D7249M
Zhang et al. [115]	2020	Performance of 3D-Printed Continuous-Carbon-Fiber-Reinforced Plastics with Pressure	PLA	CF	-	Tensile, Three-point bending	GB/T1040.1-2006, GB/T449:2005
Zhang et al. [116]	2021	Prediction of deformation and failure behavior	PLA	CF	-	Tensile, Compressive, In-plane shear, Interlaminar shear	GB/T 1447-2005, ASTM-D6641, ASTM-D3518, JC/T 773-2010

Table 3. Summary of 3D printed CFRC's mechanical properties and their processing, pre-/post-processing conditions

Authors	Matrix Material	Reinforcement Material	Fiber volume percentage	Tensile strength (MPa)	Tensile modulus (GPa)	Flexural strength (MPa)	Flexural modulus (GPa)	Pre-process	Process	Post-process
Ueda et al. [27]	Nylon	CF	35	1031	71.2	945	65.7	-	Hot-compaction roller	Hot-press
Giannakis et al. [48]	Nylon, PLA	CF	-	923	52.85509	-	-	-	-	-
Ming et al. [78]	Epoxy	CF	58	-	-	952.89	74.05	Impregnation	Printing speed, printing space, printing thickness	Curing
Hu et al. [56]	PLA	CF	25	-	-	610.092	40.13	Impregnation	Printing speed, layer thickness, printing temperature	-
Liu et al. [71]	PA6	Sized CF, virgin CF	44.1	-	-	565.8	62.1	Impregnation	hatch spacing, layer thickness, feed rate of filament	-
Hao et al. [51]	Epoxy resin	CF	-	792.8	161.4	202	143.9	-	Printing path,	Curing
Iraqi et al. [61]	Onyx	CF	27	779.8	60.9	-	-	-	Orthotropic directions	-
Hou et al. [55]	PLA	KF	50	742.6	41.3	-	-	-	Fiber contents	-
Pyl et al. [91]	Nylon	CF	27	719	58.07	-	-	-	Fiber direction	-
Justo et al. [64]	Nylon	CF GF	40 50	701.41 574.58	68.08 25.86	- -	- -	-	The direction of the fiber	-

Todoroki et al. [103]	Nylon	CF	30	701	60.9	-	-	-	Lay-up direction	-
Zhang et al. [115]	PLA	CF	10.30	644.8	-	401.24	-	-	Pressure roller	-
Shiratori et al. [98]	Nylon	CF	30	610.8	-	-	-	-	-	-
Goh et al. [49]	Nylon	CF	41	600	13	430	38.1	Impregnation	-	-
Ghebretinsae et al. [47]	Onyx	CF	42	559.9	۲۵	۲۷۰/۷	۱۶/۴	-		-
Van Der Klift et al. [105]	Nylon	CF	34.5	520	35.7	-	-	-	-	-
Dutra et al. [45]	Nylon	CF	32.8	493.9	45.2	-	-	-	-	-
Akhoundi et al. [17]	PLA	GF	49.3	479	29.4	-	-	Impregnation	Fiber-volume percentage	-
Chacon et al. [35]	Nylon	CF GF KF	26.38 27.13 27.13	436.7 381.2 305.2	51.7 19.6 25.5	423.5 205.1 189.8	39.2 16.2 14.1	-	Build orientation, layer thickness, fiber volume content	-
Mohammadizadeh et al. [80]	Nylon	CF GF KF	58 28 43	404.3 372.1 309.14	- - -	- - -	- - -	-	Fiber type, fiber orientations, temperatures	-
Hedayati et al. [52]	PCL	PGA suture	22	380	79.7	3.5	-	-	Lay-down pattern	-
Tian et al. [102]	PLA	CF	27	-	-	335	30	-	Temperature, layer thickness, hatch spacing, feed rate of the filament, printing speed	-

Dong et al. [41]	Nylon	KF	90	333.143	27	-	-	-	Fiber orientation, volume fraction, the position of fibers	-
Naranjo-Lozada et al. [84]	Nylon	CF	54	304.28	-	-	-	-	Infill density, infill patterns, fiber volume fraction, the printing architecture	-
Akhoundi et al. [28]	PLA	GF	30.5	234	19.4	-	-	-	Nozzle system	-
	PLA+	GF	31.5	268	19.7	-	-			
	PLA-wood	GF	33.6	270	19.9	-	-			
	TPU	GF	34.8	227	18.2	-	-			
	HDglass	GF	31.3	285	19	-	-			
	POM	GF	37.5	267	21.5	-	-			
	PA+CF	GF	36.3	234	20.8	-	-			
Ming et al. [77]	Epoxy	GF	43	272.51	8.01	299.36	8.35	Impregnation	UV curing	Heat treatment
Yu et al. [113]	Onyx	CF	48.72	-	-	270.63	-	-	Infill pattern	-
Tian et al. [101]	PLA	CF	8.9	256	20.6	263	13.3	Recycled impregnated filament	-	-
Peng et al. [87]	PLA	CF	19.1	-	-	261.7	16	-	Raster angle, stacking sequence, loading direction	-

Araya-Calvo et al. [29]	Onyx	CF	48.93	-	-	231.1	14.17	-	Print orientation, percentage of fiber	-
			32.19	-	-	143.3	8.89			
			17.18	-	-	83.5	5.16			
Oztan et al. [86]	PLA, Nylon	CF	14.1	254.8	-	-	-	-	-	-
		KF	16.7	150.2	-	-	-			
Chen et al. [37]	PLA	GF	45	241	-	313	21.5	Impregnation	Nozzle diameter, edge width, layer thickness, printing speed, temperature	-
Wang et al. [108]	Pb50Sn50	Cu-CF	45.75	236.7	-	-	-	Impregnation	Printing speed, temperature	-
Sanei et al. [95]	Onyx	CF	15	224	21.1	-	-	-	-	-
Dickson et al. [39]	Nylon	CF	11	216	7.73	250.23	13.02	-	Fiber orientation, fiber type, volume fraction	-
		GF	10	206	3.75	196.75	4.21			
		KF	10	164	4.37	125.80	6.65			
Bettini et al. [32]	PLA	Aramid	8.6	203	9.34	-	-	-	Feed, deposition rate, deposition path	-
Zhang et al. [116]	PLA	CF	5.9	190.1	-	142.7	-	Surface modification, ultrasonic treatment	Structural anisotropy, along 1, 2, and 3 directions	-
Matsuzaki et al. [74]	PLA	CF	6.6	185.2	19.5	-	-	Impregnation	-	-
		JF	6.1	57.1	5.11	-	-			

Wang et al. [109]	PLA	GF	۵٫۲۱, 6.24	171.66	-	148	-	-	Printing temperature, speed, layer height, fiber volume fraction	-
Vaneker et al. [106]	polypropylene (PP)	GF	-	-	-	-	13.06	-	The cutting device, modified deposition strategy	-
Qiao et al. [92]	PLA	CF	5	164.8	3.2	174.4	9.2	Impregnation with ultrasonic treatment	-	-
Yang et al. [110]	ABS	CF	10	147	4.185	127	7.72	-	-	-
Luo et al. [73]	PLA	CF	40	143.11	4.05	-	-	Preparation process	-	-
Chen et al. [38]	Onyx	CF	8.036	136	1.276	-	-	-	Average and central mode structures	-
Prajapati et al. [88]	Onyx	GF	30.1	126.1	-	-	-	-	-	-
		HSHT GF	30.1	131	-	-	-			
Ipekci et al. [60]	photopolymer	GF	-	125	-	450	14.5	-	Nozzle diameter, printing speed, fiber density, and ultraviolet (UV) light intensity	-
Mosleh et al. [82]	ABS	CF	11.4	119.85	-	102.6	-	Impregnation	Nozzle diameter,	-

									layer height, print speed	
Chaudhry et al. [36]	PLA	CF	1.7	112	0.97	164	8.528	-	Number of layers, material impact, interlayer gap	-
Yin et al. [112]	PLA	CF	9.62	111	12.2	152.9	9.5	-	Number of layers, hatch space, filling angle	-
Mei et al. [75]	Nylon	CF GF KF	-	110 91 75	3.941 1.826 2.044	-	-	-	Fiber layers, infill pattern	-
Gonzalez-Estrada et al. [50]	Nylon	CF GF	-	104 83	4.431 1.61	- -	- -	-	Fiber orientation, infill density & pattern, reinforcement distribution	-
Prajapati et al. [90]	Onyx	HSHT GF	30	94.2	-	-	-	-	-	-
Li et al. [68]	PLA	CF	34	91	-	156	-	Surface preprocessing modification	Extrusion nozzle, printing path control	-
Shi et al. [97]	Nylon	KF	8.43	88.18	-	-	-	-	Layer distributions, fiber orientations	-
Dong et al. [42]	PLA	KF	16.32	87.36		-	-	-	Cell length, layer thickness	-

Liu et al. [69]	PA6, Carbon nanotube (CNT), graphene nano platelet (GNP)	KF	1% GNP	80.4	-	-	-	-	Nanofillers	-
Heidari-Rarani et al. [53]	PLA	CF	28.2	61.4	8.28	152.1	13.42	Fiber surface preparation	Innovative extruder, printing temperature, feed rate	-
Baumann et al. [31]	ABS	CF GF	0.3 0.6	41 49	۲ ۲٫۰۵	- -	- -	-	Implementing fibers	-
Mori et al. [81]	ABS	CF	1.6	43	-	-	-	-		
Cersoli et al. [34]	PLA	KF	20.53	84.1	3.68	84.9	2.68	-	Fiber volume fraction	-
Yao et al. [111]	PLA	CF	-	32.570	-	68.211	-	CFs impregnated with DY-E44 resin	-	-
Shang et al. [26]	PLA	CF	15	32.1	3.347	-	-	-	Amplitude & frequency of structural parameters	-

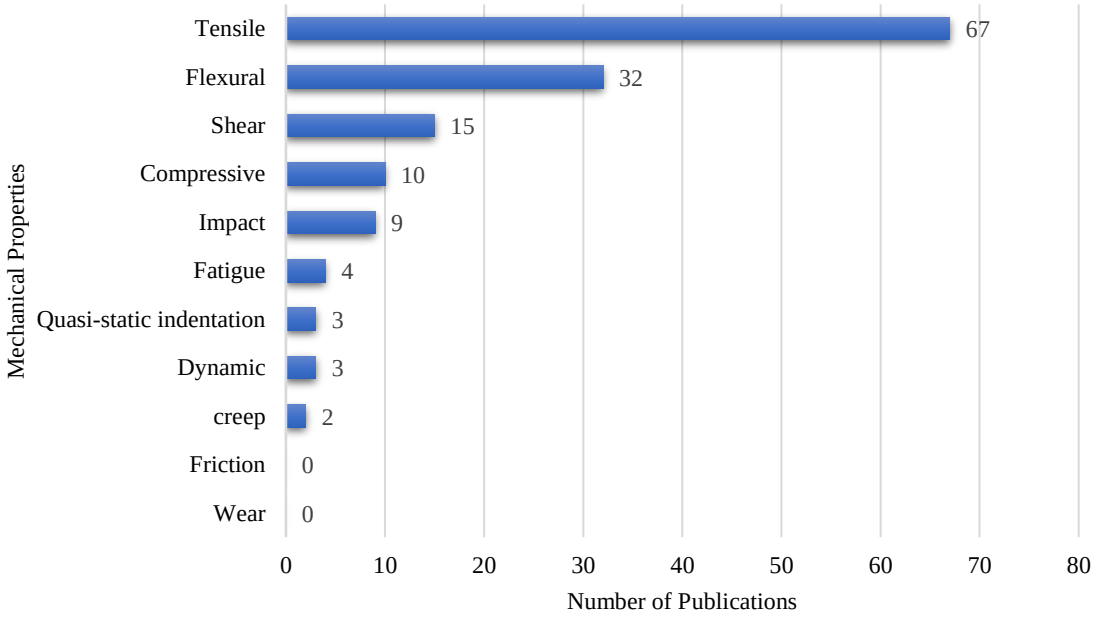

Fig. 6 Various mechanical characteristics, and the number of publications that have examined them

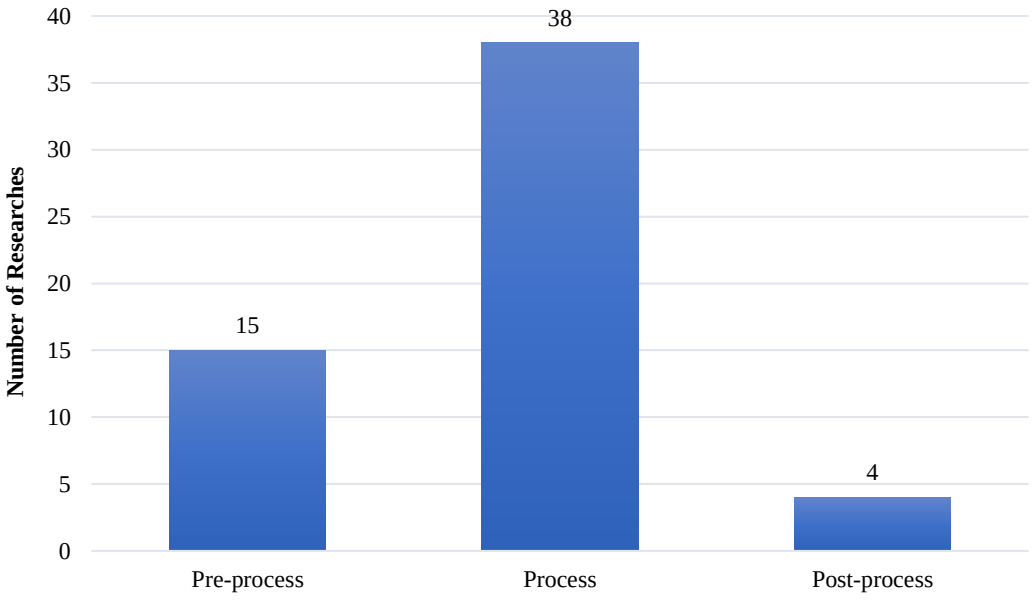

Fig. 7 Number of researches done on Pre-process, process, and postprocessing of CFRCs

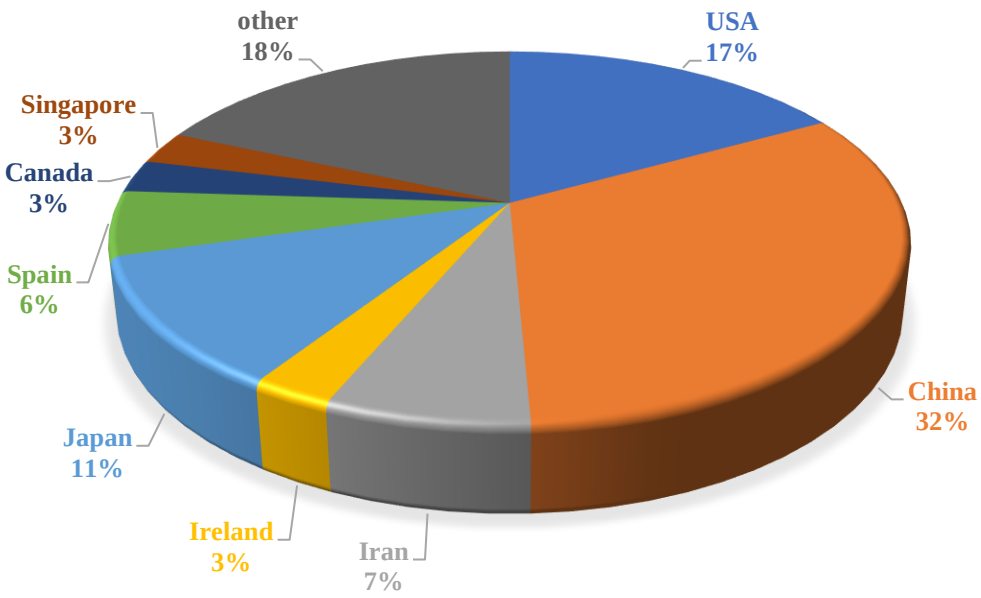

Fig. 8 Published articles in the field of CFRC 3D printing by country

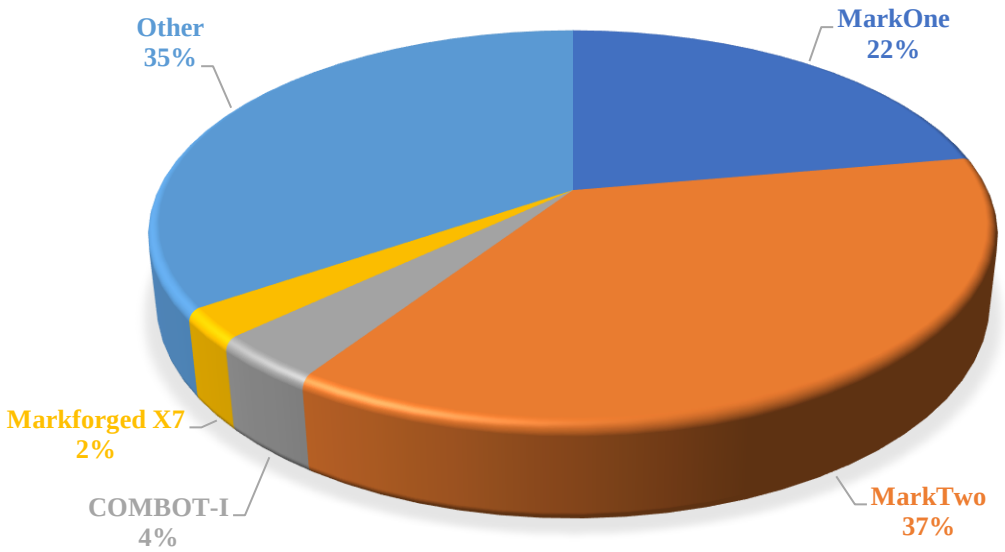

Fig. 9 Printers used for 3D printing of CFRCs

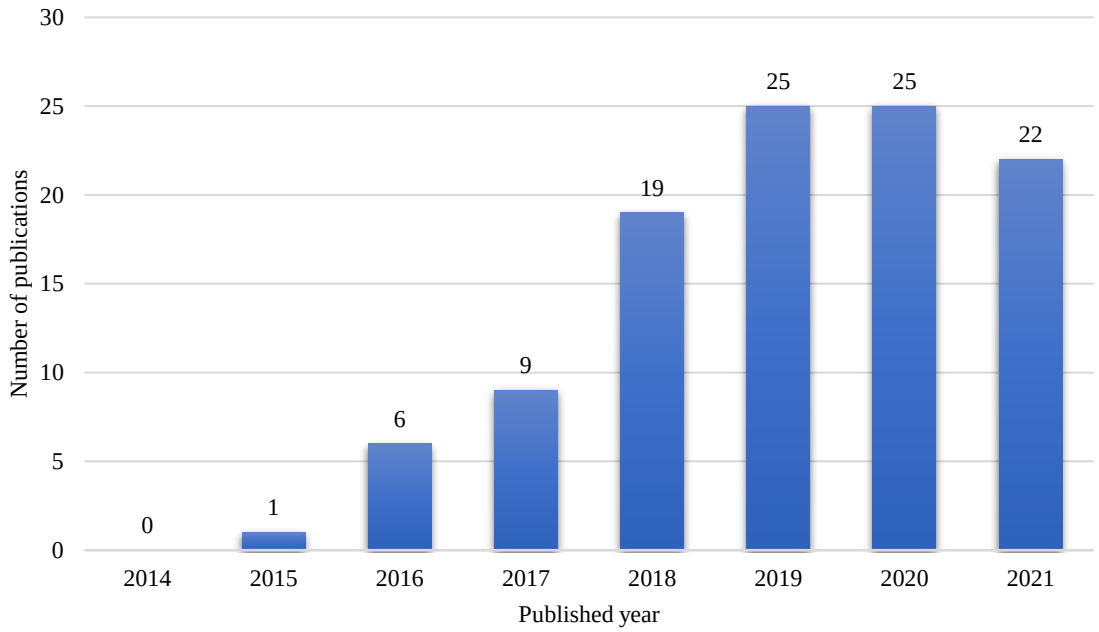

Fig. 10 Number of CFRC 3D printing articles published each year

6. Pre-processing conditions

6.1. Impregnation

As indicated in

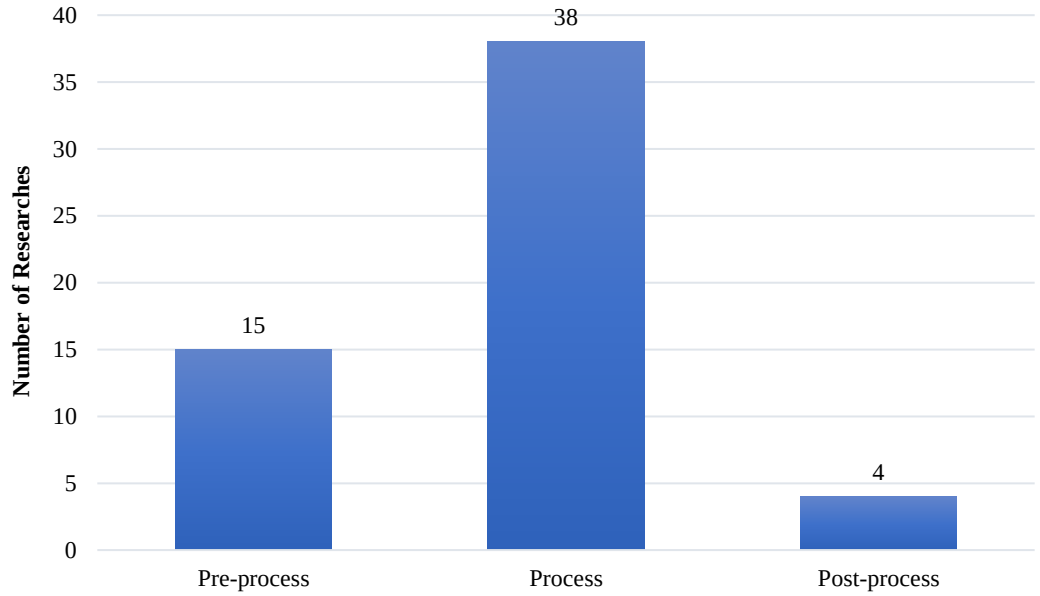

Fig. *7*, pre-processing was the subject of 15 of the papers evaluated (mostly on impregnation). The application of impregnation is shown schematically in Fig. 11. The findings revealed that impregnation quality has a significant impact on mechanical characteristics.

(a)

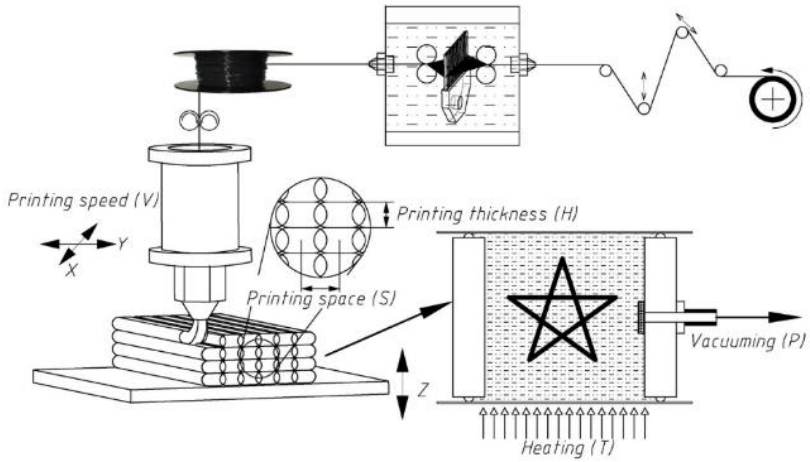
Printing speed (V)
Printing thickness (H)
Printing space (S)
Vacuuming (P)
Heating (T)
Y
X
Z

(b)

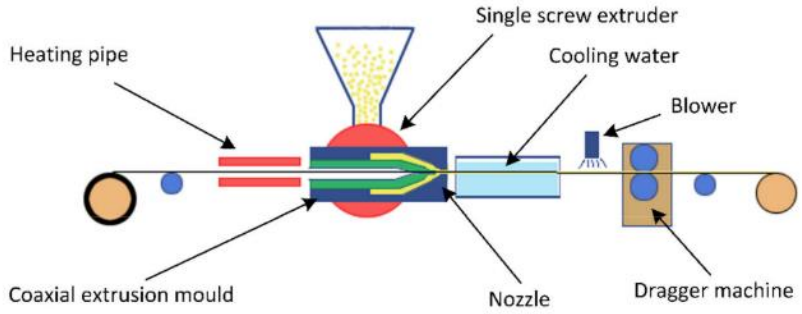
Heating pipe
Single screw extruder
Cooling water
Blower
Coaxial extrusion mould
Nozzle
Dragger machine

(c)

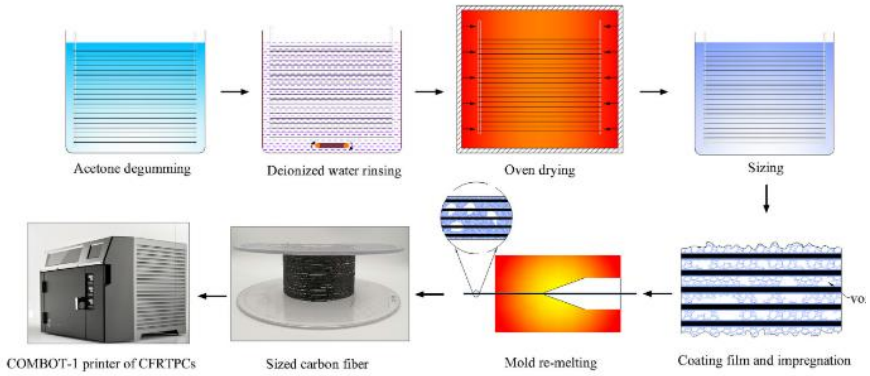
Acetone degumming
Deionized water rinsing
Oven drying
Sizing
COMBOT-1 printer of CFRTPCs
Sized carbon fiber
Mold re-melting
Coating film and impregnation

(d)

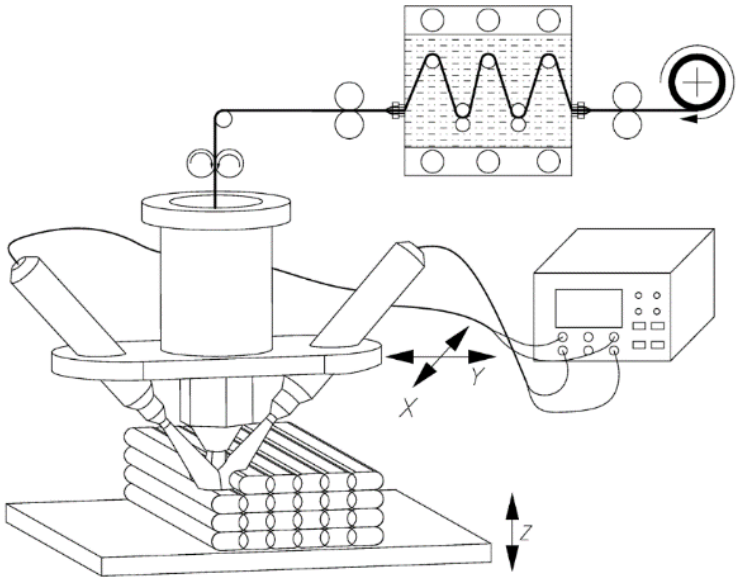
Y
X
Z

(e)

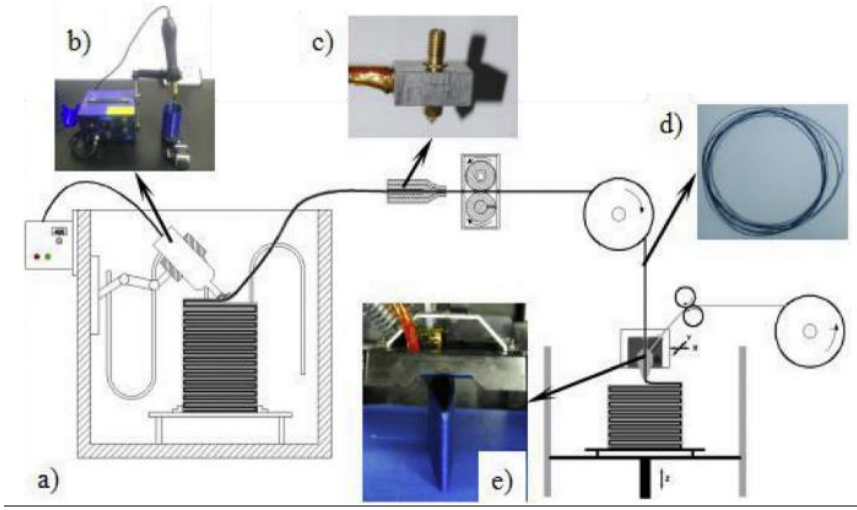
b)
c)
d)
a)
e)

(f)

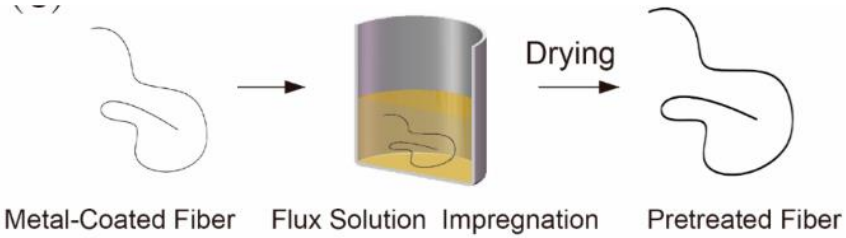
Drying
Metal-Coated Fiber
Flux Solution
Impregnation
Pretreated Fiber

(g)

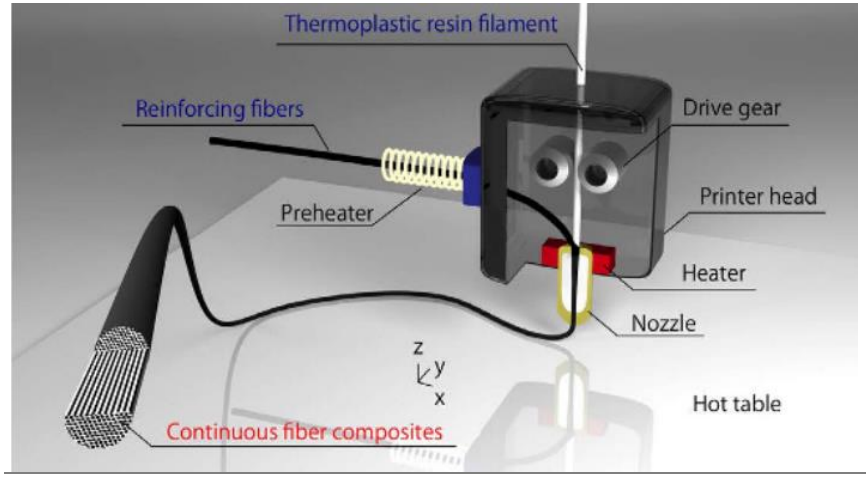
Thermoplastic resin filament
Reinforcing fibers
Drive gear
Preheater
Printer head
Heater
Nozzle
z
y
x
Hot table
Continuous fiber composites

(h)

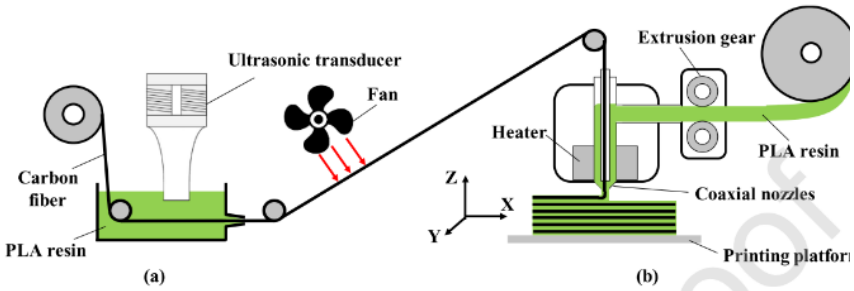
Ultrasonic transducer
Fan
Carbon fiber
PLA resin
(a)
Extrusion gear
Heater
PLA resin
Z
X
Y
Coaxial nozzles
(b)

(i)

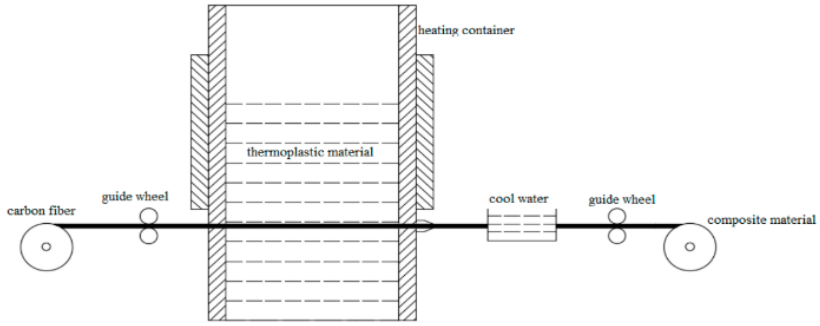
heating container
thermoplastic material
carbon fiber
guide wheel
cool water
guide wheel
composite material

(j)

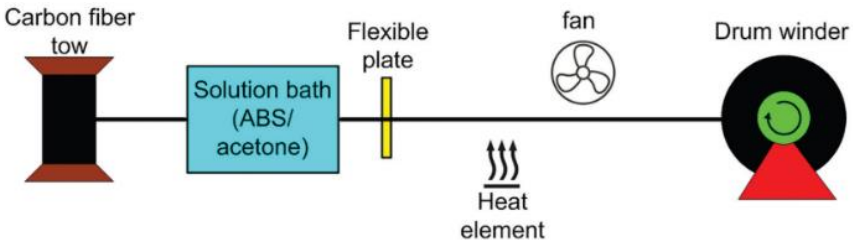
Carbon fiber tow
Solution bath (ABS/ acetone)
Flexible plate
fan
Drum winder
Heat element

(k)

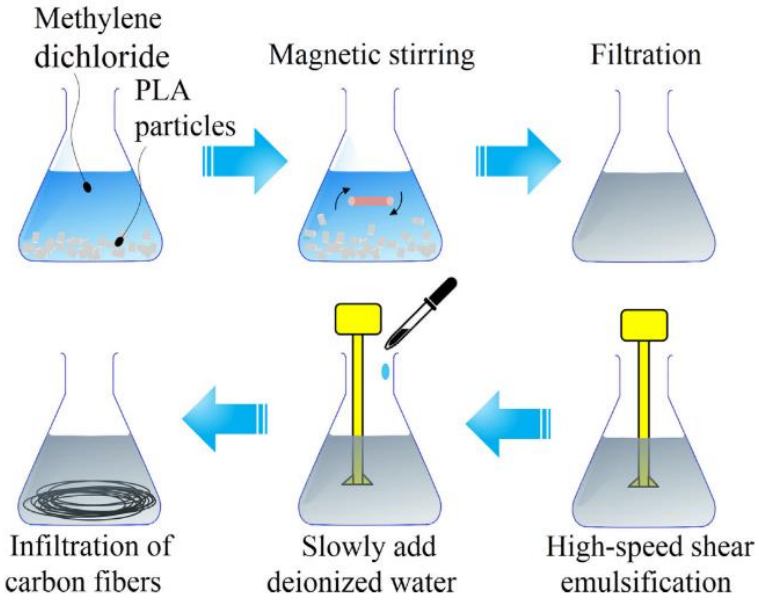
Methylene dichloride
PLA particles
Magnetic stirring
Filtration
Infiltration of carbon fibers
Slowly add deionized water
High-speed shear emulsification

(l)

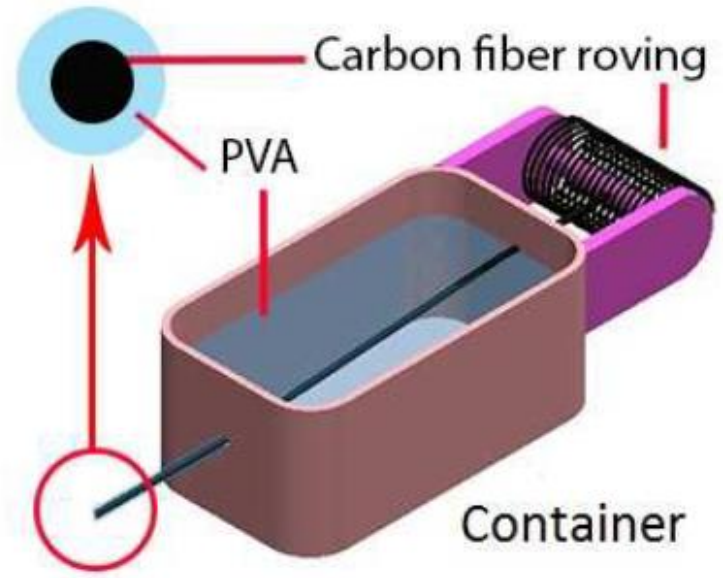
Carbon fiber roving
PVA
Container

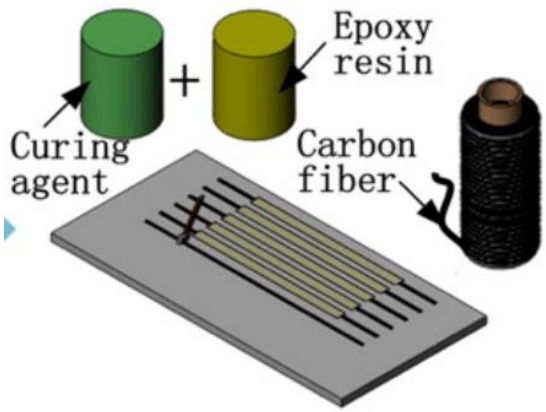

(m)

Fig. 11 Different simultaneous impregnation systems. (a) Ming et al. [78], (b) Hu et al. [56], (c) Liu et al. [71], (d) Ming et al. [77], (e) Tian et al. [101], (f) Wang et al. [108], (g) Matsuzaki et al. [74], (h) Qiao et al. [92], (i) Luo et al. [73], (j) Mosleh et al. [82], (k) Li et al. [68], (l) Heidari-Rarani et al. [53], and (m) Yao et al. [111]

By impregnating 3K CFs with the thermosetting matrix at 130°C, Ming et al. [78] created the required 3D printing filament. Because various deflections along the impregnation path and adjustment of the conveying tension may enhance the impregnation area, the method used many yarn rollers and spreading needles to stretch the fibers for a greater impregnation result (see Fig. 11(a)). To make the continuous CF prepreg filament, Hu et al. [56] used a single screw extruder and coaxial extrusion molds. The liquid resin has a higher pressure because of the single screw extruder, which may compress the molten resin into the continuous CF filaments in the nozzle. Apart from guaranteeing that the resin is readily squeezed into the filaments, the coaxial extrusion mold, particularly its nozzle, also generates a resin barrier to protect the inner continuous CF filament. The continuous CF was heated in the heating pipe before entering the coaxial extrusion mold to keep it dry and warm and guarantee that the filaments are readily saturated with the molten resin. After impregnation, the continuous CF prepreg filament was placed in cooling water to solidify, and a fan was employed to maintain the filament dry in the next phase. The dragger machine provided the necessary power to keep the entire production process running smoothly (see Fig. 11(b)).

According to Liu et al. [71], the virgin CF was first extracted with acetone for 48 hours, then repeatedly rinsed with deionized water and dried in an oven at 100°C for 2 hours to remove the original epoxy sizing layer. The CF was then immersed in the aqueous PA845H solution for 12 hours to guarantee that the polyamide solids penetrated the fiber bundle completely. Following that, the CF was aired at room temperature while polyamide particles were deposited on each fiber surface to produce a sizing film, and some polyamide solids were also present between fibers to form pre-impregnation. The distribution of polyamide solids, on the other hand, was uneven, with some gaps in the fiber bundle and a rough visible surface. As a result, a remolding nozzle with a

diameter of 0.4 mm suggested a melt impregnation procedure. The pre-impregnated CF was continually pushed through the nozzle at a speed of 10 mm/s, while the polyamide solids were melted at 200 °C to mix and fill the gaps in the nozzle under pressure to achieve uniform distribution and a smooth surface. Finally, the CFRCs method employed sized CF and PA6 filament as raw materials to build composite components using a 3D printer (see Fig. 11(c)). The procedure was easy and cheap, and it enhanced the interlaminar shear strength of the PA6/sized CF sample by 42.2%.

Ming et al. [77] used a thermosetting matrix with a low viscosity of 1.3 Pa.s (Pascal-second) at 130°C to impregnate continuous glass fibers (GFs). In the molten resin tank, many yarn rollers were used to stretch the fiber bundles and guarantee a broad resin impregnation area. The stretched fiber bundles were then molded into a cylinder form using a squeezing nozzle, the excess resin scraped off, and the impregnated continuous GFs extruded through a squeezing nozzle (see Fig. 11(d)). Tian et al. [101] presented a recycling and remanufacturing method for 3D printed CFRC. From 3D printed composite components, continuous CF and PLA matrix were recycled in the form of PLA impregnated CF filament. With the action of the hot air cannon, they softly and consistently took out the CF. The impregnated CF filament with a somewhat rough surface was produced by resolidified thermoplastic material adhering to the fiber (see Fig. 11(e)). Due to enhanced surface characteristics, impregnated recycled continuous CF has a greater tensile strength (142 N) than the original printed filament (118 N).

Wang et al. [108] submerged the Cu/CF in flux solution for 1 minute before drying it at ambient temperature (25°C). Matsuzaki et al. [74] heated the reinforcing fibers with a nichrome wire before introducing them into the nozzle to improve the permeation of the fiber bundles with thermoplastic resin; the heat diffuses to the resin, lowering the PLA viscosity. Drive gears and a stepping motor

transport the resin filament, while reinforcing fibers are sent directly to the nozzle. The reinforcing fibers are automatically fed to the head by the movement of the resin filament, thus no extra equipment is necessary for feeding them. The heater within the printer head melts the resin filament, merging the reinforcing fibers and resin in the heated area.

By dissolving the thermoplastic resin in dichloromethane, Qiao et al. [92] created a resin solution. The CF bundle is then dragged into the resin solution pool by the winding machine. The CF bundle maintains a constant tension throughout the movement thanks to the rotating dampers (as shown in Fig. 11(a)). The CF bundle is 10 mm away from the ultrasonic transducer and entirely immersed in the resin solution. Following that, under the cavitation of the ultrasonic transducer, the resin solution penetrates deeper into the CF bundle. The impregnated CF bundle is then passed through a scraping hole to scrape off any extra resin on its surface, and the dichloromethane solvent is volatilized under hot air. Finally, as a printing raw material, the pretreated CF bundle is wound on the winding machine reel. The resin solution pool is kept sealed throughout the operation to prevent solvent evaporation, the ultrasonic transducer is kept cold with flowing water to prevent resin sticking, and the CF solvent evaporation process is carried out in the fume hood (see Fig. 11(h)). The influence of ultrasonic pretreatment parameters such as amplitude, resin solution concentration, and treatment speed on the mechanical characteristics of printed components has been investigated. The results show that when the amplitude increases, the tensile strength, and elastic modulus rise first, then fall. The tensile and flexural strength and modulus reach their maximum when the amplitude is 40 μm, resulting in tensile strength and modulus of 164.8 MPa and 3.2 GPa, respectively. The tensile strength and the tensile and flexural modulus of the material rose as the percentage of resin solution concentration increased. Strength, tensile, and flexural modulus decrease as treatment speed rises.

The dry CF tow was run through the whole preparation apparatus by Luo et al. [73]. The PLA particles are then heated to a molten state at 210°C in a sealed container. At the same temperature, the two materials are combined. They will then travel at a speed of 10 mm/s through a 0.6 mm nozzle. Finally, they are chilled in room temperature water (25°C) to produce a CCF PLA composite material (see Fig. 11(i)). Mosleh et al. [82] developed solution impregnated fibers (prepregs). In a closed vessel at room temperature, 8 g ABS was swirled in 100 mL acetone for 30 minutes. To avoid compatibility concerns, the impregnation solution was made with the same ABS grade printing filament. A drum winder was used to draw the CF through the solution bath. To remove the surplus solution from prepregs, a flexible plate with a certain hole size was employed (Fig. 11(j)). The findings demonstrate that impregnation before printing enhances mechanical characteristics and simplifies 3D printing.

PLA particles (8 percent mass fraction) were introduced to a methylene dichloride solution by Li et al. [68]. After 30 minutes of magnetic stirring, the PLA particles were partly dissolved. The DE-100LB high-speed dispersion and emulsification machine shears and emulsifies the PLA resin filtrate in methylene dichloride solution at 8000 revolutions per minute. With a 1 percent mass fraction of the whole solution, the surface-active, emulsifying, and antifoaming agents are added to the deionized water. The deionized water is then progressively added to process the aqueous PLA sizing agent to change the surface condition of the CFs (see Fig. 11(k)). The tensile and flexural strengths of modified CFRCs were 13.8% and 164% greater than the original CF reinforced samples, according to the data. The modified CF reinforced samples had a storage modulus that was 166% and 351% greater than the PLA and original fiber reinforced samples, respectively.

Heidari-Rarani et al. [53] dissolved roughly 400g water-soluble polyvinyl alcohol (PVA) in 2 L water in a container and impregnated CF roving in this solution for 1 hour at 60°C. The impregnated roving is passed through a die with a 1 mm hole and dried at room temperature to remove the excess PVA and create an approximate circular cross-section (see Fig. 11(l)). For the CF preparation, Yao et al. [111] impregnated a 250 mm length of fiber with a two-component (1:1) DY-E44 epoxy resin adhesive.

7. Process (printing) conditions

Similar to 3D printing of neat thermoplastics, the quality of 3D printed CFRCs is influenced by a variety of variables. The bulk of CFRC 3D printing research has focused on printing (processing) parameters rather than pre- and post-processing conditions (see

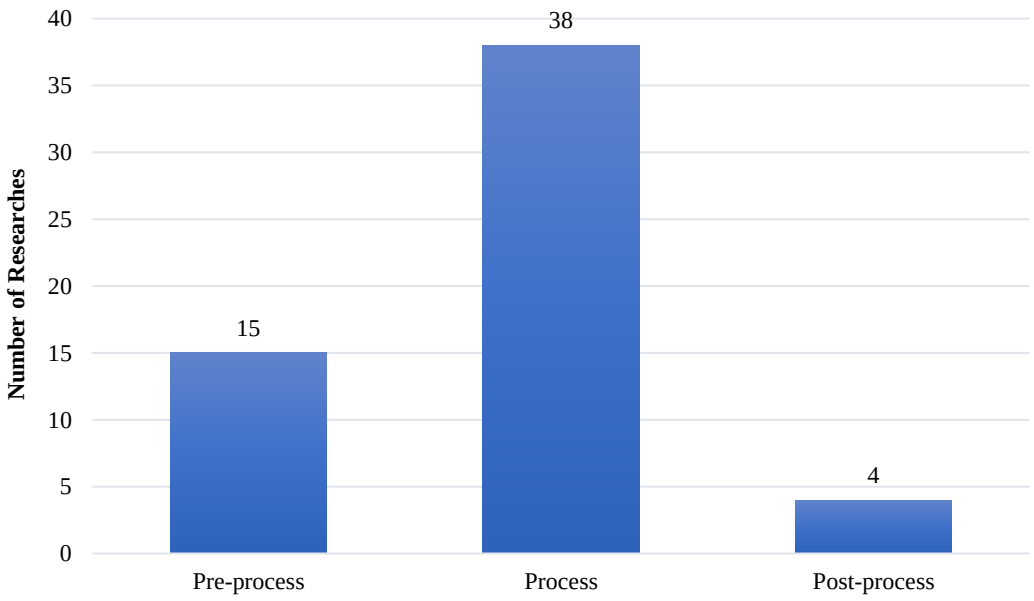

Fig. *7*). Process factors can have a significant influence on mechanical properties, according to the literature. Table 3 outlines the procedures utilized in the literature, with a focus on tensile and flexural testing. Fig. 12 depicts the investigated process variables. Each of these variables will be discussed in more detail.

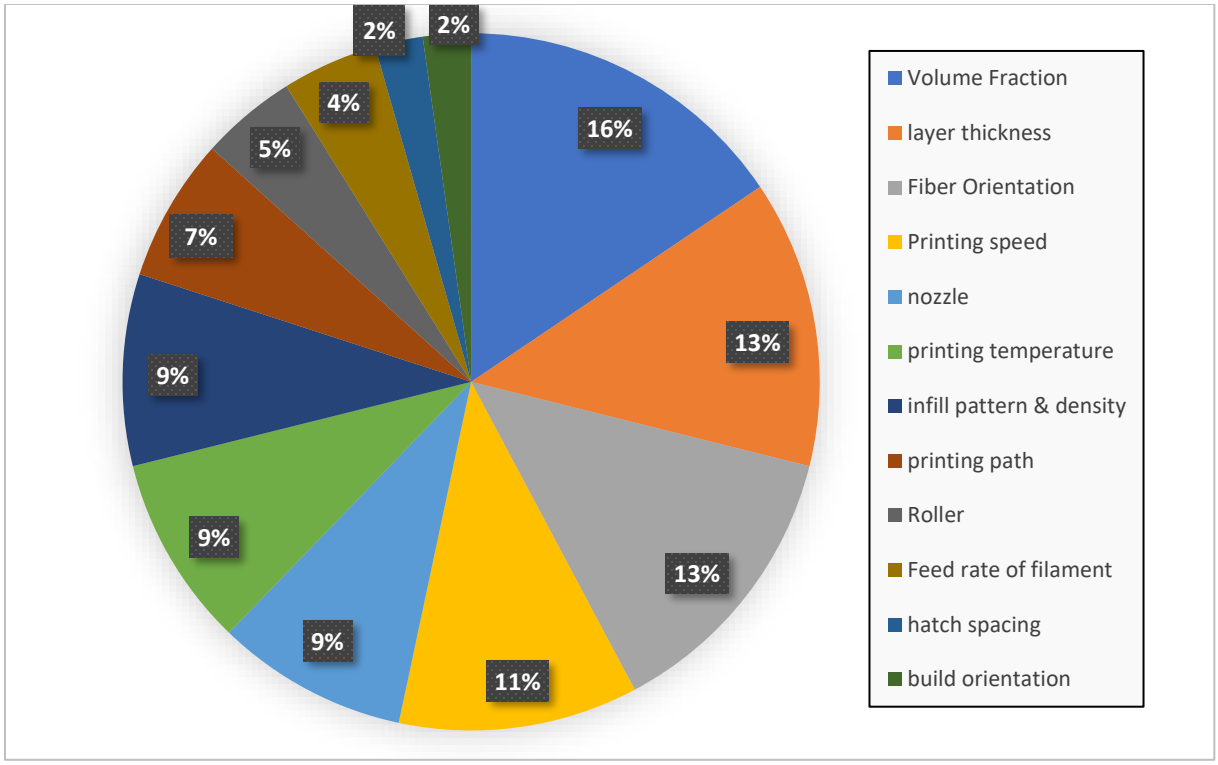

Fig. 12 Processing (printing) parameters assessed in the literature

7.1. Fiber Volume Fraction

The fiber volume fraction (FVF) of CFRCs, as well as their tensile and flexural strength and modulus, are listed in Table 3. To further understand the relationship between the fraction of FVF and the mechanical properties of CFRCs, the data in Table 3 is presented in Fig. 13 and Fig. 14.

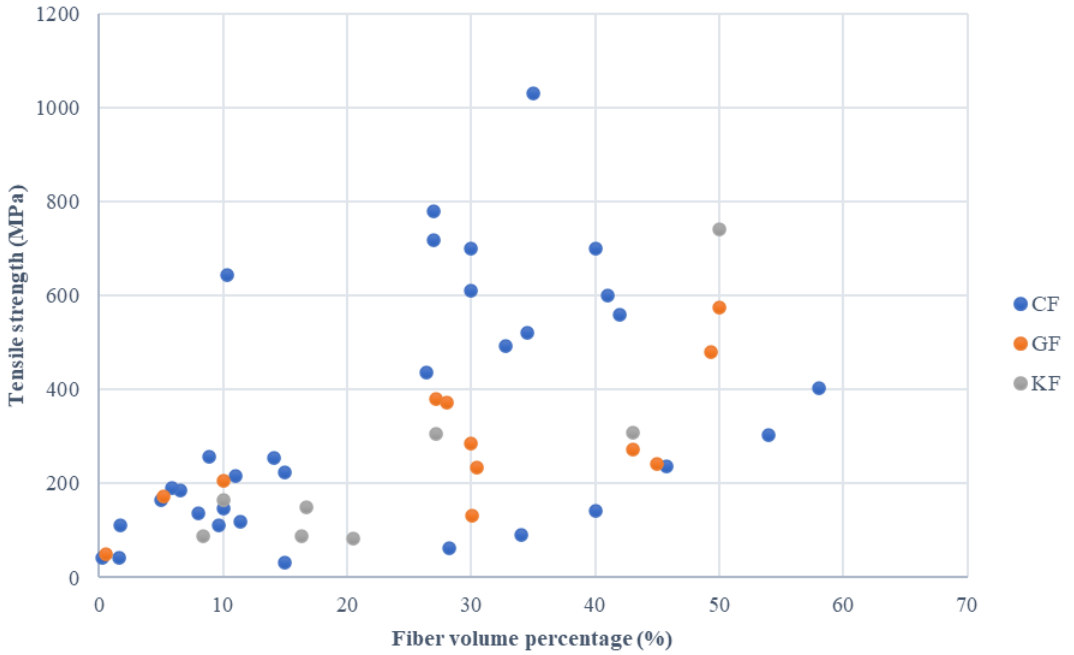

Fig. 13 Relation between FVF and Tensile Strength

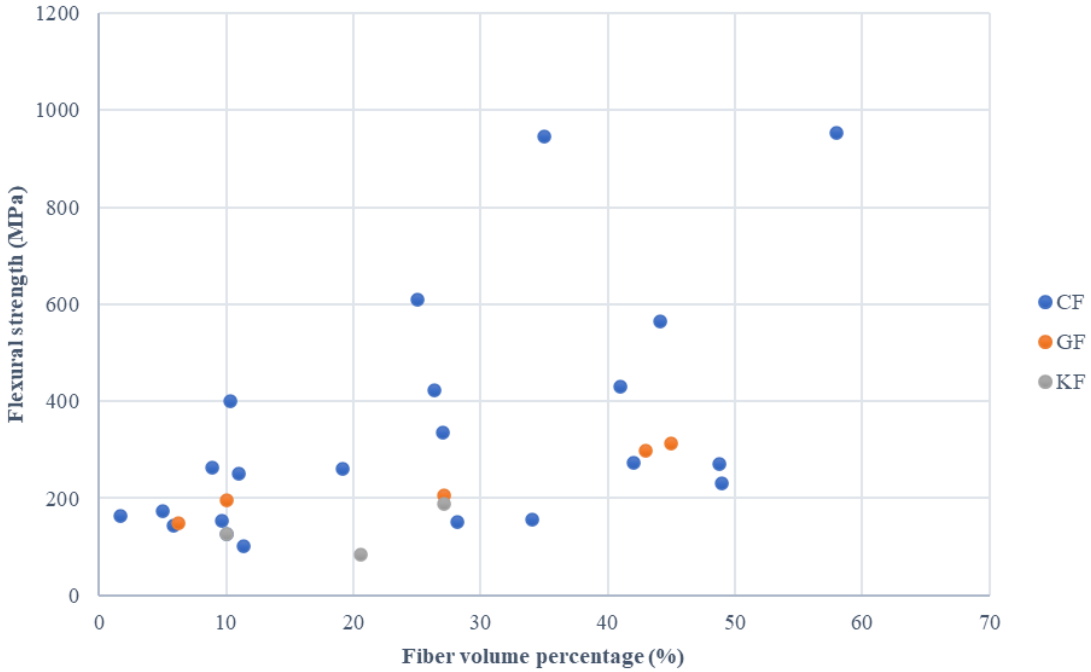

Fig. 14 Relation between FVF and Flexural Strength

Hou et al. [55] investigated the mechanical characteristics of PLA/Kevlar composites with different fiber volume contents (6.7, 10, 12.5, 20, 30, 40, 50 percent). The findings reveal that increasing the fiber volume content of the samples from 6.7 to 50% improves longitudinal tensile strength from 141.8 MPa to 742.6 MPa, but decreases transverse tensile strength, longitudinal compressive strength, transverse compressive strength, and in-plane shear strength. Furthermore, if the fiber volume content of the samples is increased by 40%, the longitudinal tensile and compressive moduli will increase to 41.3 GPa and 5.89 GPa, respectively. These moduli do not rise by a further increase of the fiber volume content increases from 40% to 50%.

R3, R4, R5, and R6 were the four samples examined by Akhoundi et al. [17], with fiber volumes of 49.3, 46.3, 40.18, and 35.14 percent, respectively. The results show that as the percentage of fiber volume increases, the tensile strength and tensile modulus increase, with tensile strengths of 479 MPa, 446 MPa, 401 MPa, and 333 MPa for samples R3, R4, R5, and R6, and tensile modulus of 29.41 GPa, 27.76 GPa, 24.31 GPa, and 21.9 GPa for samples R3, R4, R5, and R6, respectively.

Chacon et al. [35] used continuous carbon, glass, and Kevlar fibers as reinforcing material in printed nylon matrix composites. The fiber volume content of the samples varied from 1.88 to 27.13 percent for each of the reinforcing fibers. The results show that as the fiber volume content of the samples increases, so does their tensile and flexural strength. For example, when the fiber volume content of the samples changes from 1.88 to 27.13, the tensile strength improves from 96.6 MPa to 436.7 MPa, and the strength bending improves from 80.7 MPa to 423.5 MPa, and the tensile modulus increases from 7.6 GPa to 51.7 GPa, and the flexural modulus increases from 6.1 GPa to 39.2 GPa.

The impact of fiber volume content in nylon/CF composites was studied by Naranjo-Lozada et al. [84]. The samples' fiber volume fractions are 4, 7, 11, 32, and 54 percent, respectively. The results reveal that samples with a greater fiber volume percentage had higher strength and tensile modulus.

For PA6/CF composites, Araya-Calvo et al. [29] conducted bending tests on samples with 17.18, 32.19, and 48.93 percent fiber volume fraction, as well as compression testing on samples with 8.18, 16.59, and 24.44 percent. The modulus and proportional limit of bending and compression have grown as the amount of reinforcement have increased. The proportional limit of bending for the samples is 83.5 MPa, 143.3 MPa, and 231.1 MPa, respectively. The samples' bending moduli are 5.16 GPa, 8.89 GPa, and 14.17 GPa, respectively.

Dickson et al. [39] investigated the impact of FVF on the mechanical performance of a nylon matrix composite reinforced with carbon, glass, and Kevlar fibers. Volume fractions of 4, 9, 13.5, 18, 22.5, 27, and 33 percent were used to make the composites. The results show that when the FVF of the samples is increased from 4 to 13.5, the strength of the sample is increased by 516 percent. but when the volume fraction is increased to 33, the strength of the sample volume fraction increases by 13.5 percent, or 516 percent. By increase of the volume fraction of samples from 13.5 to 33 percent, 44 percent increase in strength occurred, resulting in maximum flexural strength of 444 MPa.

Cersoli et al. [34] looked at how fiber volume fraction affected PLA/Kevlar composites. The volume fractions of the samples are 0, 3.46, 4.74, and 20.53 percent, with the findings indicating that the greater the volume fraction, the higher the tensile strength and flexibility.

Wang et al. [109] printed composites with various fiber volume percentages, finding that the higher the fiber volume fraction, the better the mechanical characteristics.

As demonstrated in Fig. 13 and Fig. 14, as well as the reviewed publications, raising the volume fraction improves mechanical characteristics and is a very effective factor that may boost tensile and flexural strength up to 800 MPa. Furthermore, the minimum volume fraction necessary to achieve a tensile strength greater than 600 MPa is 25% in all but one of the articles. However, this is not the only factor that improves mechanical characteristics, and other aspects in the process parameters that will be discussed in the following sections will have an impact on this improvement.

7.2. Printing parameters

Layer thickness, printing speed, printing temperature, hatch spacing, and filament flow rate are all critical factors that influence mechanical qualities [102]. These five factors are nicely represented in Fig. 15. The effect of these five variables on the mechanical characteristics of composites will be discussed in the following sub-sections.

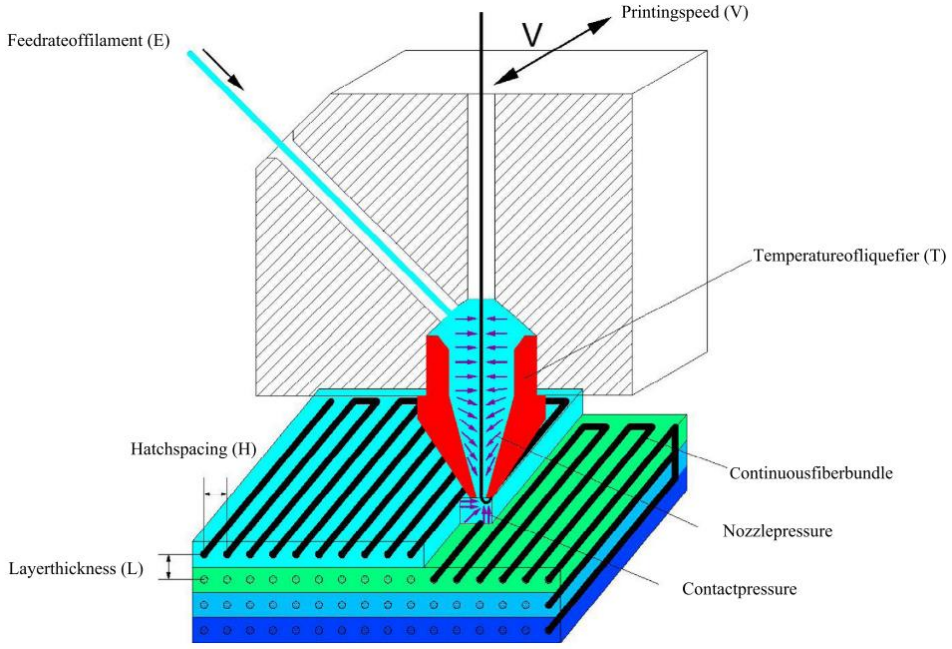

Fig. 15 Schematic of process parameters for 3D printing of CFR PLA composites [102]

7.2.1. Layer thickness

The number of layers required to print the item is directly connected to the layer thickness, which in turn is directly related to the printing time. As a result, increasing layer thickness lowers manufacturing costs. Layer thickness is a key parameter in the 3D printing process, as it affects manufacturing accuracy, interfacial bonding, performance, and mechanical characteristics of manufactured samples.

Ming et al. [78] printed samples with layer thicknesses of 0.25, 0.3, 0.35, 0.4, and 0.45 mm, respectively. The results indicated that when the layers are 0.4 mm thick, the samples' strength and flexural modulus achieve their maximum value. Because the fibers are scratched and broken when the layer thickness is less than 0.4 mm, and when the layer thickness is greater than 0.4 mm, the space between the layers becomes wider.

Hu et al. [56] printed composites with layer thicknesses of 0.6, 0.9, and 1.2 mm, and found that the lower the sample thickness, the higher the flexural strength of the samples. Chacon et al. [35] printed composites with 0.1, 0.125, and 0.2 mm layer thicknesses. The influence of layer thickness on mechanical characteristics is minor, as evidenced by the results. Tian et al. [102] used layer thicknesses of 0.3, 0.4, 0.5, 0.6, 0.7, and 0.8 mm to print composites. The findings reveal that when the thickness of the sample layer was increased, the flexural strength fell substantially, and flexural strength of 240 MPa was reached with a layer thickness of 0.3 mm. The flexural strength of the specimens falls somewhat as the layer thickness increases from 0.4 to 0.6 mm, then significantly with layer thicknesses of 0.7 and 0.8 mm. Wang et al. [109] printed samples with 0.2, 0.25, and 0.3 mm layer thicknesses. The results demonstrate that the mechanical characteristics improve as the layers become thinner.

Chen et al. [37] used varied layer thicknesses of 0.5, 0.6, 0.7, and 0.8 mm to print different samples. The authors found that increasing layer thickness lowers flexural strength and modulus, as well as impact and interlayer shear strength. The composite samples' flexural, impact, and interlayer shear strengths were the greatest at 328 MPa, 155 kJ/m^2, and 14.0 MPa, respectively, when the layer thickness was 0.5 mm. The layer thicknesses used by Dong et al. [42] were 0.1, 0.2, 0.3, 0.4, and 0.5 mm. The results reveal that as the layer thickness increased, the fiber content of the samples declined significantly, from 16.32 to 3.65 %, as did density and tensile strength, which fell from 669 to 597.54 kg/m^3 and 87.36 to 27.37 MPa, respectively. The density increased by around 12% (72 kg/m^3) when the layer thickness was reduced from 0.5 to 0.1 mm, while the tensile strength increased by 219.2 % (59.99 MPa).

To summarize, the mechanical characteristics of a layer with a smaller layer thickness are superior. However, decreasing the sample thickness lengthens the printing time. As a result, an optimal thickness value must be determined that gives acceptable mechanical characteristics and a reasonable printing time.

7.2.2. Printing speed

Samples were printed at speeds of 200, 500, 800, 1100, and 1400 mm/min by Ming et al. [78]. The results show that when the printing speed is increased from 200 to 500 mm/min, the flexural strength and modulus remain constant. However, raising the printing speed from 500 to 1400 mm/min considerably reduces the flexural strength.

Hu et al. [56] printed samples at speeds of 60, 90, and 120 mm/min. The results demonstrate that print speed has a minor impact on the samples. Printing speeds of 100, 200, 300, 400, 500, and 600 mm/min were used by Tian et al. [102]. The effects of printing speed on the mechanical characteristics of the samples are insignificant, as shown by the results. Samples were printed at

speeds of 2, 3, 4, 5, and 6 mm/s by Chen et al. [37]. The results show that as the printing speed is increased, all of the mechanical characteristics that are evaluated decrease. Samples were printed at rates of 1, 2, 3, 4, and 5 mm/s by Wang et al. [108]. The tensile strength increases as the print speed increases then drop to a maximum of 236.7 MPa at a speed of 3 mm/s.

Wang et al. [109] used speeds of 300, 400, 500, 600, 700, and 800 mm/min to print samples. The thermoplastic material may be fully connected to the bottom matrix material at printing speeds of 300, 400, and 500 mm/min. The quality of the printed corners degrades as the speed increases, but when the speed reaches 400 or 500 mm/min, the quality of the printed samples is good, and this value is also chosen for printing due to the high efficiency of 500 mm/min.

Ipekci et al. [60] printed samples at speeds of 300, 600, 900, and 1200 mm/min using photopolymer reinforced with continuous fiberglass. The results revealed that when the printing speed increases from 300 to 600 mm/s, the tensile strength improves only a little, and as the printing speed goes further, the mechanical characteristics deteriorate. As a result, 600 mm/s was an appropriate speed for the material produced in this study.

In conclusion, the printing speed can impact the filament retention time in the extruder head as well as the resin melting rate, and if the printing speed is low, the bond between the filament and the continuous reinforcing fiber will be better. As printing speed rises, the time that filament spends in the nozzle decreases, reducing pressure and impregnation time. In most studies, increasing printing speed resulted in a loss in mechanical characteristics, whereas in others, the influence of print speed on mechanical properties was shown to be insignificant.

7.2.3. Printing temperature

Temperature is a significant factor in composites manufacturing because it influences the impregnation of reinforcing fibers and matrices. The melting temperature in the printer head is also crucial for bonding printed pathways and layers in the 3D printing process. Hu et al. [56] printed samples at 200, 215, and 230 degrees Celsius. The results demonstrate that temperature has a negligible influence on the samples.

Printing samples at 180, 190, 200, 210, 220, 230, and 240 °C was done by Tian et al. [102]. The results show that as the temperature rises, the flexural strength and modulus increase, with the flexural strength and modulus at 240°C being 155 MPa and 8.6 GPa, respectively. The sample produced at 240°C, on the other hand, lost its surface precision due to PLA melt overflow. As a result, the printer's maximum suggested temperature is 230 °C, at which the produced composite samples' flexural strength and modulus were 145 MPa and 8.6 MPa, respectively. The ideal process temperature was between 200 and 230 degrees Celsius.

Chen et al. [37] printed samples at temperatures of 190, 200, 210, 220, and 230 degrees Celsius. According to the findings, boosting the temperature enhanced all of the studied mechanical characteristics. However, when the printing temperature surpasses 210°C, it becomes difficult to maintain the sample's dimensional stability, particularly at the edges. As a result, 210°C has been chosen as the optimal printing temperature.

Wang et al. [108] printed samples at temperatures of 255, 265, 275, and 285 degrees Celsius. The tensile strength of samples printed at 265 and 275°C was equivalent and maximal, according to the data. These two samples have tensile strengths of 236.7 and 233.4 MPa, respectively. Furthermore, at 265°C, the tensile modulus reached a high of 33.15 GPa. Because of the visible flaws, the composite produced at 285°C is regarded as less desirable.

Wang et al. [109] printed composites at 170, 180, 190, 200, 210, and 220 degrees Celsius. The composite printed at 210° C had the best aesthetic and quality attributes, according to the results.

In conclusion, when the printing temperature rises, so do the mechanical characteristics. Because the molten filament forms a stronger connection with the produced composite as the printing temperature rises. However, printed composites lose their aesthetic characteristics and dimensional precision at extremely high temperatures. As a result, a temperature should be chosen that preserves the part's appearance and dimensional accuracy while still providing acceptable mechanical characteristics.

7.2.4. Hatch spacing

Tian et al. [102] used hatch spacing of 0.4, 0.6, 0.8, 1, 1.2, 1.4, 1.6, and 1.8 mm to print composites. The average flexural strength increased from 130 to 335 MPa and the flexural modulus improved from 6.26 to 30 GB when hatch spacing was reduced from 1.8 to 0.4 mm.

7.2.5. Feed rate of the filament

The filament feed rate is proportional to the amount of material supplied into the printing head per unit volume. The feed rate of the filament determines the inner pressure and extrusion speed of melt material via the printing head when the tip diameter of the extrusion nozzle is the same [102].

At rates of 30, 55, 70, and 80 mm/min, Liu et al. [71] fed filaments into the 3D printer's extruder head. The flexural strength of the sample fed at a rate of 55 mm/min rose by 15% when compared to the sample fed at a rate of 70 mm/min, resulting in flexural strength of 504.58 MPa for the sample fed at 50 mm/min and 437.76 MPa for the sample fed at 70 mm/min. When the feed rate is set to 30 mm/min, however, the enhancing impact decreases because the limited amount of resin materials used resulted in low forming pressure and poor interfacial performance. The sample fed

at 80 mm/min had nearly the same flexural strength as the sample fed at 70 mm/min. Furthermore, no improvement occurred because the forming pressure was so high that overfilled resin materials caused the interfacial performance to become excessively strong, resulting in brittle fracture.

Feed rates of 60, 80, 100, 120, 140, and 160 mm/min were employed by Tian et al. [102]. The results showed that raising the feeding speed from 60 to 80 mm/min greatly increased flexural strength. Due to the large unit volume of extruded materials, which formed the dual interfaces between fiber and matrix, as well as deposited lines in the 3D printed CFR composites. This could be caused by an increase in inner pressure in the liquefier and overlapping contact pressure between adjacent deposited lines. However, as the feed rate was increased, the flexural strength did not improve, most likely due to the short fiber impregnation period.

In summary, mechanical properties improve as the feed rate of the filament increases to some extent. The mechanical properties remain constant as the feed rate of the filament increases further. More study, however, is required to better understand the influence of feed rate on the mechanical characteristics of CFRCs.

7.2.6. Fiber orientation

The fibers can be printed in two ways, as shown in Fig. 16, concentric and isotropic. They can be printed at varied angles (0, ±45, 90 degrees, see Fig. 17) in the isotropic form.

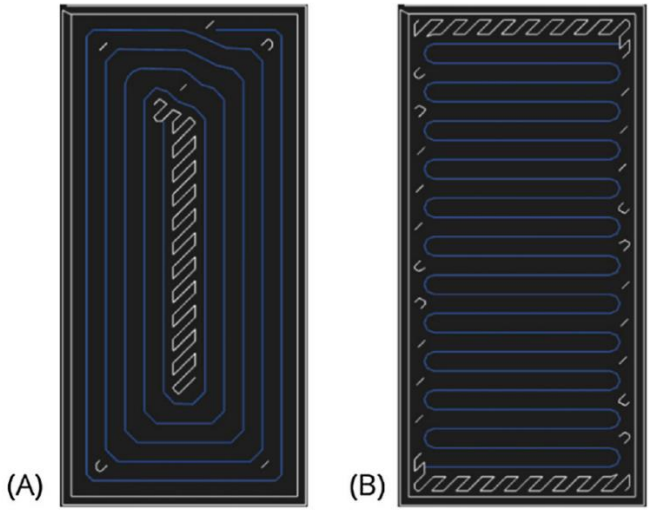

Fig. 16 Fiber reinforcement configuration, (A) concentric, and (B) isotropic – 0 degree [29]

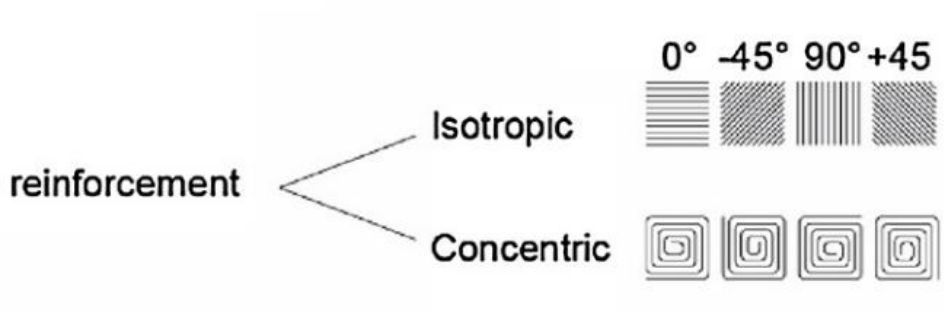

Fig. 17 Fiber orientations in a single layer [29]

In printing nylon/CF composites, Pyl et al. [91] adjusted the fiber orientations of the composites to 0 unidirectional, 0/90, 0/90/± 45, and ±45 degrees. According to the findings, composites with the fiber orientations of 0 unidirectional, 0/90, 0/90/± 45, and ±45 degrees had the highest tensile strength in that order. The strain to failure of the composites printed at 0 unidirectional, 0/90/±45 degrees was nearly identical, but the strain to failure of the ± 45 degrees sample was about four times that of the others.

Printed nylon matrix composites reinforced with carbon, glass, and Kevlar fibers were produced by Mohammadizadeh et al. [80]. The samples' infill pattern was rectangular, and their fill density was 50%. In addition, the sample infill orientations were concentric and isotropic. The composites produced in an isotropic configuration showed greater mechanical qualities than those printed in a concentric configuration, according to the findings.

Concentric and isotropic infill arrangements were employed by Yu et al. [113]. Composites with a concentric infill pattern offered higher flexural strength and energy absorption than composites with an isotropic infill pattern.

Araya-Calvo et al. [29] used concentric and isotropic infill patterns to print PA6/CF composites. Compressive and flexural tests were performed. The results of these experiments revealed that composites with a concentric pattern performed better. 1.69 GPa, 40.5 MPa, 59.07 MPa, and 5.41 GPa, respectively, were the compressive modulus, proportional limit, flexural strength, and flexural modulus of these composites.

Dickson et al. [39] used carbon, glass, and Kevlar fibers to reinforce nylon matrix composites. Concentric and isotropic designs were used to print the fibers. The composites with isotropic patterns had higher tensile and flexural strength and modulus than concentric specimens. In addition, the flexural testing revealed that the concentric pattern composites perform better in bending than in tension.

Gonzalez-Estrada et al. [50] used angles of 0, 45, and 90 degrees to print nylon/GF composites. The composites printed at 0, 45, and 90 degrees had the highest strength and modulus, respectively. When compared to the 45 degree sample, the 0 degree sample has significantly better strength and modulus. Nylon/Kevlar composites with angles of 30, 45, and 60 degrees were created by Shi et

al. [97]. The lower the angle, the greater the yield stress, i.e., the highest yield stress is for 30, 45, and 60 degrees, respectively.

In conclusion, increasing the print orientation (from 0 to 90 degrees) reduces the mechanical characteristics of composites produced with the isotropic pattern. The orientation of the reinforcing fibers, on the other hand, must be 0 degrees to have high mechanical qualities. It is impossible to determine which of the isotropic and concentric patterns has higher mechanical qualities. Because in some circumstances [39, 80], an isotropic pattern gave higher mechanical qualities, whereas, in other studies [29, 113], concentric patterns were found to produce better mechanical properties.

7.2.7. Build orientation

The mechanical qualities of printed composites are also influenced by the build orientation. The composites can be built in one of three orientations, as shown in Fig. 18: flat, on-edge, and upright. Chacon et al. [35] tested nylon matrix composites reinforced with carbon, Kevlar, and glass fibers in Charpy tests. The composites were printed in two orientations: flat and on-edge (the fill density and fill pattern were 100 percent and rectangular and isotropic with zero degrees angle). The on-edge composites had higher impact strength, according to the findings.

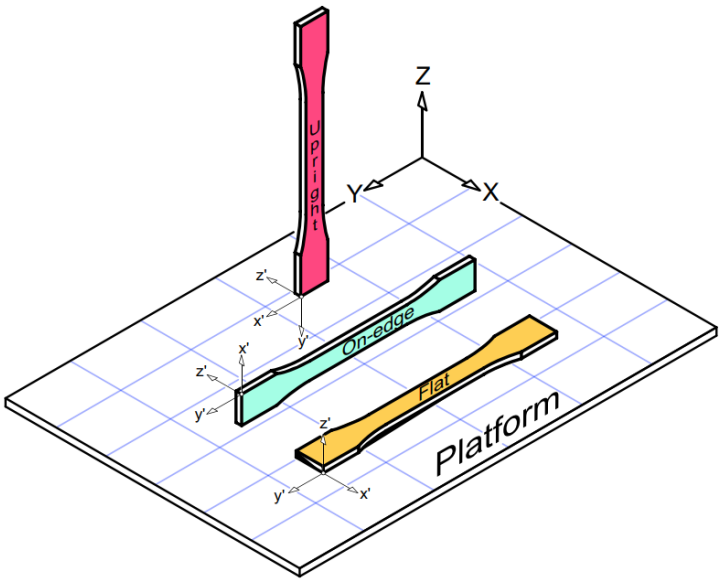

Fig. 18 Different types of build orientation [117]

7.2.8. Infill pattern & density

Naranjo-Lozada et al. [84] created Onyx/CF composites with infill densities of 10% and 70% with triangular and rectangular infill patterns. Composites with a triangle design performed better in tensile tests than those with a rectangular pattern. The modulus of elasticity improved when the infill density of the specimens was increased from 10% to 70%, but the tensile yield strength of these two composites was nearly identical.

Gonzalez-Estrada et al. [50] printed nylon/GF and nylon/CF composites with triangular, rectangular, and hexagonal infill patterns. The samples' infill density was 20% and 50%, respectively. Higher stiffness and ultimate tensile strength were achieved with the triangular pattern. Changing the infill density from 20% to 50%, on the other hand, has no noticeable impact on the properties indicated. Increasing the infill density from 20% to 50% resulted in a 3.3 percent improvement in elastic modulus and a 5.5 percent increase in tensile strength.

Printed nylon matrix composite reinforced with carbon, glass, and Kevlar fibers by Mei et al. [75]. The composite's infill patterns were rectangular, hexagonal, and triangular. The samples had the same number of concentric fiber rings and fiber layers. Rectangular infill had values of 4, 6, and 8; hexagonal infill had a value of 6, and triangular infill had a value of 6. The rectangular structure with 8 concentric fiber rings and fiber layers had the highest tensile strength and modulus, according to the data. As a result, the tensile strength and modulus increase as the number of concentric fiber rings and fiber layers increases.

According to the articles listed above, increasing the amount of infill density improves mechanical qualities slightly. In addition, the triangular, hexagonal, and rectangular infill patterns, respectively, offered the best mechanical qualities. The explanation for the rectangular sample's superiority in Mei et al. [75] is that the analyzed samples had more rims than the other samples.

7.3. Compaction roller technique

Ueda et al. [27] created two samples, one with compaction rollers and the other with the hot-pressing method. The compression roller (see Fig. 5 (d)) and the printer bed had temperatures of 270°C and 100°C, respectively. The results demonstrated that the compaction roller improves the printed composite's mechanical properties, with the printed composite having a better fracture surface than the hot press sample. The roller-made composite had a smoother surface than the hot-pressed one. The roller-made sample had a void fraction of 3%, while the hot press sample had a void fraction of 10%.

Zhang et al. [115] printed PLA/CF composites with a compaction roller (see Fig. 19). The sample's tensile and flexural strength rose with increasing pressure to 644.8 MPa and 401.24 MPa, respectively (compared to the tensile and flexural strength of specimens without pressure, which

was 109.9 MPa and 163.13 MPa, respectively). Furthermore, as the pressure is increased, the quality of the sample surface degrades, and the sample may fail.

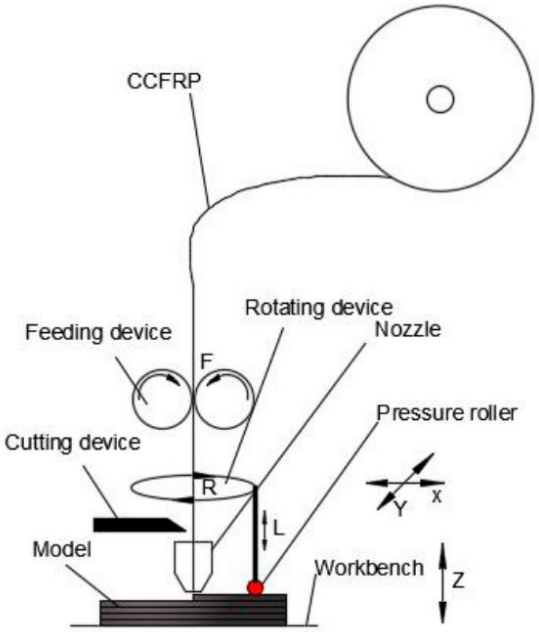

Fig. 19 Schematic of the 3D-printing machine. [115]

Based on the findings of [27, 115], it can be deduced that applying pressure during printing improves the mechanical properties greatly. Furthermore, this process has capabilities that are comparable to the hot press method.

8. Postprocessing

Postprocessing is one of the most effective approaches to improve the mechanical properties of CFRCs. Three of the four articles that performed postprocessing on their samples acquired extraordinarily high tensile and flexural strength, as shown in Table 3. The number of publications

devoted to postprocessing processes, on the other hand, is quite minimal (see

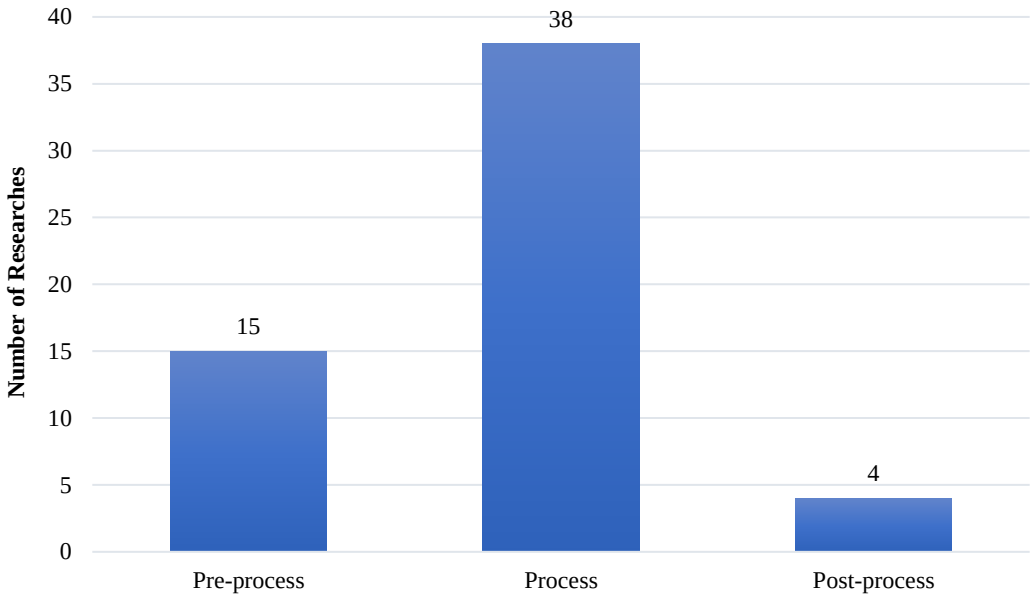

Fig. *7*). The high expenses of postprocessing activities could be one cause for this. There is a need for more research in this area, as well as the application of postprocessing to improve mechanical qualities in the future as technology advances. In what follows, a brief review of articles dedicated to CFRC postprocessing will be discussed.

As indicated in the previous section, Ueda et al. [27] used a compaction roller to make composites (see Fig. 5(d)). They also hot-pressed 3D-printed composites for 10 minutes at a temperature of 230°C and a pressure of 0.1 MPa (see Fig. 20). The sample thickness was reduced by 16 percent and the weight was reduced by 1.5 percent after hot pressing. The flexural properties of this sample were comparable to those of a compaction roller-produced sample. It can be concluded that thermal compaction rollers can be employed instead of hot pressing.

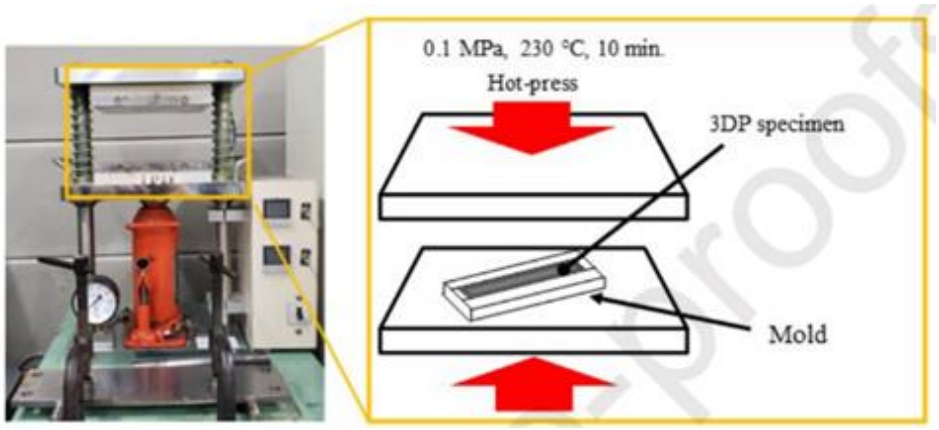

Fig. 20 Hot-press operation on reinforced composites [27]

Ming et al. [78] used a vacuum chamber to cure 3D printed materials at various curing pressures and temperatures (see Fig. 11 (a)). The specimens were first exposed to vacuum pressures of -10, -30, -50, -70, and -90 kPa. The results revealed that the higher the vacuum pressure (the more negative the pressure), the better the specimens' strength and flexural modulus. The fibers were discovered to be covered with a thin layer of resin before curing, and there were several voids inside the specimens. But after curing, the fibers were evenly covered with resin, and the interior voids were significantly reduced. Negative pressure can increase resin diffusion and fiber impregnation, according to these findings. A small pressure increase led to a significant decrease in fiber content. As a result, because it affects resin flow, void distribution, and fiber content during curing, curing pressure is a vital parameter that must be regulated. Curing temperatures of 150, 160, 170, 180, and 190 degrees Celsius were also applied to the samples. The results revealed that increasing the curing temperature from 150 to 170 degrees enhanced flexural strength and modulus to their maximum levels. On the other hand, the flexural strength and modulus decreased dramatically as the curing temperature increased from 170 to 190 degrees Celsius.

Hot pressing and vacuuming are two feasible options for postprocessing and thereby increasing the mechanical properties of CFRCs, according to the findings of these two papers. The higher negative the pressure in a vacuum system, the better the mechanical properties.

9. Suggestions

According to the previous sections' comments, a lot of topics in CFRC 3D printing are either unexplored or underexplored. These themes could be interesting and relevant research subjects in the future:

1. CFRCs have yet to be subjected to wear and friction tests.
2. A modest number of studies have been conducted on CFRC dynamic, fatigue, creep, impact, and indentation tests.
3. The impregnation and postprocessing activities should be given special attention. In addition, more research is needed to understand the impact of postprocessing factors on composite mechanical properties.
4. More research might be done on build orientation, such as printing specimens flat, on-edge, and upright, and investigating the effects on mechanical qualities.
5. The hatch spacing process parameter should be adjusted, and the impacts on mechanical qualities should be investigated.
6. More research on isotropic and concentric printed samples is needed.
7. Kevlar and glass fiber reinforced composites' bending characteristics should be investigated further. The impact of fiber volume fraction on the bending strength of these composites should be studied in particular.
8. It is necessary to evaluate the impact of specimen geometry, printing parameters, and printing patterns on printing time and specimen defects.

9. The ability to undertake post-printing procedures such as forming and machining, as well as the consequences of these operations on the features of 3D printed CFRCs, is further intriguing topics for wider use of these composites.

10.Conclusions

The majority of CFRC research employing FDM technology has been covered in this review paper. All of the parameters impacting the mechanical properties of CFRCs were evaluated. The following are the conclusions reached:

Impregnation is critical in pre-processing, and the results reveal that the higher the impregnation quality, the better the mechanical qualities. Pre-heating the fiber, applying ultrasonic vibration, and pre-impregnation inside a solution all help to increase impregnation and, as a result, improve mechanical qualities.

The following findings are drawn from examining the process (printing) parameters:

- Tensile and flexural strength and modulus rise as the fiber volume percentage increases.
- The thinner the layer thickness, the greater the mechanical qualities.
- As printing speed drops, mechanical qualities improve.
- The mechanical properties of the samples improve as the printing temperature rises, but it should be noted that as the print temperature rises, the appearance properties and dimensional precision of the samples deteriorate.
- As the quantity of hatch spacing is reduced, mechanical qualities improve.
- As the filament feed rate is raised, the mechanical characteristics improve initially and then remain constant.

- For specimens having an isotropic pattern printed on them, the lower the mechanical qualities, the larger the angle of the fibers (0 degrees provides the best mechanical properties).
- The samples with a higher percentage of infill density have slightly better mechanical properties.
- The triangular, hexagonal, and rectangular infill patterns have the best mechanical properties, respectively.
- The use of hot compaction rollers will greatly improve mechanical qualities, but extreme caution must be exercised to avoid over-pressuring the specimens.

Finally, proven postprocessing methods for improving the mechanical properties of CFRCs include hot pressing, vacuuming, and post-heat treatment.

References

1. Mazurchevici, A.D., D. Nedelcu, and R. Popa, *Additive manufacturing of composite materials by FDM technology: A review.* Indian Journal of Engineering and Materials Sciences (IJEMS), 2021. **27**(2): p. 179-192.
2. Joshi, S.C. and A.A. Sheikh, *3D printing in aerospace and its long-term sustainability.* Virtual and Physical Prototyping, 2015. **10**(4): p. 175-185.
3. Lim, C.W.J., et al., *An overview of 3-D printing in manufacturing, aerospace, and automotive industries.* IEEE potentials, 2016. **35**(4): p. 18-22.

4. Aimar, A., A. Palermo, and B. Innocenti, *The role of 3D printing in medical applications: a state of the art.* Journal of healthcare engineering, 2019. **2019**.
5. Ventola, C.L., *Medical applications for 3D printing: current and projected uses.* Pharmacy and Therapeutics, 2014. **39**(10): p. 704.
6. Cai, H., *Application of 3D printing in orthopedics: status quo and opportunities in China.* Annals of translational medicine, 2015. **3**(Suppl 1).
7. Nicholas, P., et al., *Integrating real-time multi-resolution scanning and machine learning for Conformal Robotic 3D Printing in Architecture.* International Journal of Architectural Computing, 2020. **18**(4): p. 371-384.
8. Mathur, R., *3D printing in architecture.* International Journal of Innovative Science, Engineering & Technology, 2016. **3**(7): p. 583-591.
9. Balletti, C., M. Ballarin, and F. Guerra, *3D printing: State of the art and future perspectives.* Journal of Cultural Heritage, 2017. **26**: p. 172-182.
10. Liu, Z., et al., *3D printing: Printing precision and application in food sector.* Trends in Food Science & Technology, 2017. **69**: p. 83-94.
11. Derossi, A., et al., *Application of 3D printing for customized food. A case on the development of a fruit-based snack for children.* Journal of Food Engineering, 2018. **220**: p. 65-75.
12. Godoi, F.C., S. Prakash, and B.R. Bhandari, *3d printing technologies applied for food design: Status and prospects.* Journal of Food Engineering, 2016. **179**: p. 44-54.
13. Vanderploeg, A., S.-E. Lee, and M. Mamp, *The application of 3D printing technology in the fashion industry.* International Journal of Fashion Design, Technology and Education, 2017. **10**(2): p. 170-179.

14. Spahiu, T., et al. *On the possible use of 3D printing for clothing and shoe manufacture*. in *Proceedings of the 7th International Conference of Textile, Tirana, Albania*. 2016.

15. Spahiu, T., E. Canaj, and E. Shehi, *3D printing for clothing production.* Journal of Engineered Fibers and Fabrics, 2020. **15**: p. 1558925020948216.

16. Bikas, H., P. Stavropoulos, and G. Chryssolouris, *Additive manufacturing methods and modelling approaches: a critical review.* The International Journal of Advanced Manufacturing Technology, 2016. **83**(1-4): p. 389-405.

17. Akhoundi, B., A.H. Behravesh, and A. Bagheri Saed, *Improving mechanical properties of continuous fiber-reinforced thermoplastic composites produced by FDM 3D printer.* Journal of Reinforced Plastics and Composites, 2019. **38**(3): p. 99-116.

18. Al Abadi, H., et al., *Elastic properties of 3D printed fibre-reinforced structures.* Composite Structures, 2018. **193**: p. 8-18.

19. Arif, M., et al., *Performance of biocompatible PEEK processed by fused deposition additive manufacturing.* Materials & Design, 2018. **146**: p. 249-259.

20. Wang, X., et al., *3D printing of polymer matrix composites: A review and prospective.* Composites Part B: Engineering, 2017. **110**: p. 442-458.

21. Kabir, S.F., K. Mathur, and A.-F.M. Seyam, *A critical review on 3D printed continuous fiber-reinforced composites: History, mechanism, materials and properties.* Composite Structures, 2020. **232**: p. 111476.

22. Crump, S., *Apparatus and method for creating three-dimensional objects (US Patent US5121329A).* 1989.

23. Bryll, K., et al. *Polymer composite manufacturing by FDM 3D printing technology*. in *MATEC Web of Conferences*. 2018. EDP Sciences.

24. Sanei, S.H.R. and D. Popescu, *3D-Printed carbon fiber reinforced polymer composites: a systematic review*. Journal of Composites Science, 2020. **4**(3): p. 98.

25. Wickramasinghe, S., T. Do, and P. Tran, *FDM-based 3D printing of polymer and associated composite: A review on mechanical properties, defects and treatments.* Polymers, 2020. **12**(7): p. 1529.

26. Shang, J., et al., *Controllable inter-line bonding performance and fracture patterns of continuous fiber reinforced composites by sinusoidal-path 3D printing.* Composites Science and Technology, 2020. **192**: p. 108096.

27. Ueda, M., et al., *3D compaction printing of a continuous carbon fiber reinforced thermoplastic.* Composites Part A: Applied Science and Manufacturing, 2020. **137**: p. 105985.

28. Akhoundi, B., A.H. Behravesh, and A. Bagheri Saed, *An innovative design approach in three-dimensional printing of continuous fiber–reinforced thermoplastic composites via fused deposition modeling process: in-melt simultaneous impregnation.* Proceedings of the Institution of Mechanical Engineers, Part B: Journal of Engineering Manufacture, 2020. **234**(1-2): p. 243-259.

29. Araya-Calvo, M., et al., *Evaluation of compressive and flexural properties of continuous fiber fabrication additive manufacturing technology.* Additive Manufacturing, 2018. **22**: p. 157-164.

30. Vinoth Babu, N., et al., *Influence of slicing parameters on surface quality and mechanical properties of 3D-printed CF/PLA composites fabricated by FDM technique.* Materials Technology, 2021: p. 1-18.

31. Baumann, F., J. Scholz, and J. Fleischer, *Investigation of a new approach for additively manufactured continuous fiber-reinforced polymers.* Procedia Cirp, 2017. **66**: p. 323-328.

32. Bettini, P., et al., *Fused deposition technique for continuous fiber reinforced thermoplastic.* Journal of Materials Engineering and Performance, 2017. **26**(2): p. 843-848.

33. Caminero, M., et al., *Impact damage resistance of 3D printed continuous fibre reinforced thermoplastic composites using fused deposition modelling.* Composites Part B: Engineering, 2018. **148**: p. 93-103.

34. Cersoli, T., et al., *3D printing of a continuous fiber-reinforced composite based on a coaxial Kevlar/PLA filament.* Composites and Advanced Materials, 2021. **30**: p. 26349833211000058.

35. Chacón, J., et al., *Additive manufacturing of continuous fibre reinforced thermoplastic composites using fused deposition modelling: Effect of process parameters on mechanical properties.* Composites science and technology, 2019. **181**: p. 107688.

36. Chaudhry, F.N., et al., *Effect of carbon fibre on reinforcement of thermoplastics using FDM and RSM.* Journal of Thermoplastic Composite Materials, 2019: p. 0892705719886891.

37. Chen, K., et al., *Optimization of printing parameters of 3D-printed continuous glass fiber reinforced polylactic acid composites.* Thin-Walled Structures, 2021. **164**: p. 107717.

38. Chen, W., et al., *Process evaluation, tensile properties, mathematical models, and fracture behavior of 3D printed continuous fiber reinforced thermoplastic composites.* Journal of Reinforced Plastics and Composites, 2021: p. 07316844211016091.

39. Dickson, A.N., et al., *Fabrication of continuous carbon, glass and Kevlar fibre reinforced polymer composites using additive manufacturing.* Additive Manufacturing, 2017. **16**: p. 146-152.

40. Dikshit, V., et al., *Quasi-static indentation analysis on three-dimensional printed continuous-fiber sandwich composites.* Journal of Sandwich Structures & Materials, 2019: p. 1099636219836058.

41. Dong, G., et al., *Mechanical properties of continuous kevlar fiber reinforced composites fabricated by fused deposition modeling process.* Procedia Manufacturing, 2018. **26**: p. 774-781.

42. Dong, K., et al., *Mechanical properties and shape memory effect of 4D printed cellular structure composite with a novel continuous fiber-reinforced printing path.* Materials & Design, 2021. **198**: p. 109303.

43. Dong, K., et al., *3D printing of continuous fiber reinforced diamond cellular structural composites and tensile properties.* Composite Structures, 2020. **250**: p. 112610.

44. Dugbenoo, E., et al., *Enhanced Bonding via Additive Manufacturing-Enabled Surface Tailoring of 3D Printed Continuous-Fiber Composites.* Advanced Engineering Materials, 2018. **20**(12): p. 1800691.

45. Dutra, T.A., et al., *Mechanical characterization and asymptotic homogenization of 3D-printed continuous carbon fiber-reinforced thermoplastic.* Journal of the Brazilian Society of Mechanical Sciences and Engineering, 2019. **41**(3): p. 1-15.

46. Fernandes, R.R., A.Y. Tamijani, and M. Al-Haik, *Mechanical characterization of additively manufactured fiber-reinforced composites.* Aerospace Science and Technology, 2021. **113**: p. 106653.

47. Ghebretinsae, F., O. Mikkelsen, and A. Akessa. *Strength analysis of 3D printed carbon fibre reinforced thermoplastic using experimental and numerical methods*. in *IOP Conference Series: Materials Science and Engineering*. 2019. IOP Publishing.

48. Giannakis, E., et al., *Static and fatigue properties of 3D printed continuous carbon fiber nylon composites.* Int. J. Mod. Manuf. Technol, 2019. **11**: p. 69-76.

49. Goh, G.D., et al., *Characterization of mechanical properties and fracture mode of additively manufactured carbon fiber and glass fiber reinforced thermoplastics.* Materials & Design, 2018. **137**: p. 79-89.

50. González-Estrada, O.A., A. Pertuz, and J.E. Quiroga Mendez. *Evaluation of tensile properties and damage of continuous fibre reinforced 3D-printed parts*. in *Key Engineering Materials*. 2018. Trans Tech Publ.

51. Hao, W., et al., *Preparation and characterization of 3D printed continuous carbon fiber reinforced thermosetting composites.* Polymer Testing, 2018. **65**: p. 29-34.

52. Hedayati, S.K., et al., *3D printed PCL scaffold reinforced with continuous biodegradable fiber yarn: A study on mechanical and cell viability properties.* Polymer Testing, 2020. **83**: p. 106347.

53. Heidari-Rarani, M., M. Rafiee-Afarani, and A. Zahedi, *Mechanical characterization of FDM 3D printing of continuous carbon fiber reinforced PLA composites.* Composites Part B: Engineering, 2019. **175**: p. 107147.

54. Hetrick, D.R., et al., *Charpy impact energy absorption of 3D printed continuous Kevlar reinforced composites.* Journal of Composite Materials: p. 0021998320985596.

55. Hou, Z., et al., *A constitutive model for 3D printed continuous fiber reinforced composite structures with variable fiber content.* Composites Part B: Engineering, 2020. **189**: p. 107893.

56. Hu, Q., et al., *Manufacturing and 3D printing of continuous carbon fiber prepreg filament.* Journal of materials science, 2018. **53**(3): p. 1887-1898.

57. Hu, Y., et al., *Carbon fibre damage during 3d printing of polymer matrix laminates using the fdm process.* Materials & Design, 2021: p. 109679.

58. Ibrahim, Y., et al., *Effective thermal conductivity of 3D-printed continuous fiber polymer composites.* Advanced Manufacturing: Polymer & Composites Science, 2020. **6**(1): p. 17-28.

59. Imeri, A., et al., *Fatigue analysis of the fiber reinforced additively manufactured objects.* The International Journal of Advanced Manufacturing Technology, 2018. **98**(9): p. 2717-2724.

60. İpekçi, A. and B. Ekici, *Experimental and statistical analysis of robotic 3D printing process parameters for continuous fiber reinforced composites.* Journal of Composite Materials, 2021: p. 0021998321996425.

61. Iragi, M., et al., *Ply and interlaminar behaviours of 3D printed continuous carbon fibre-reinforced thermoplastic laminates; effects of processing conditions and microstructure.* Additive Manufacturing, 2019. **30**: p. 100884.

62. Ishii, K., et al., *Bending fracture rule for 3D-printed curved continuous-fiber composite.* Advanced Composite Materials, 2018.

63. Jahangir, M., et al., *Reinforcement of material extrusion 3D printed polycarbonate using continuous carbon fiber.* Additive Manufacturing, 2019. **28**: p. 354-364.

64. Justo, J., et al., *Characterization of 3D printed long fibre reinforced composites.* Composite Structures, 2018. **185**: p. 537-548.

65. Kabir, S.F., K. Mathur, and A.-F.M. Seyam, *Impact resistance and failure mechanism of 3D printed continuous fiber-reinforced cellular composites.* The Journal of The Textile Institute, 2020: p. 1-15.

66. Kousiatza, C., D. Tzetzis, and D. Karalekas, *In-situ characterization of 3D printed continuous fiber reinforced composites: A methodological study using fiber Bragg grating sensors.* Composites Science and Technology, 2019. **174**: p. 134-141.

67. Li, H., et al., *The quantitative analysis of tensile strength of additively manufactured continuous carbon fiber reinforced polylactic acid (PLA).* Rapid Prototyping Journal, 2019.

68. Li, N., Y. Li, and S. Liu, *Rapid prototyping of continuous carbon fiber reinforced polylactic acid composites by 3D printing.* Journal of Materials Processing Technology, 2016. **238**: p. 218-225.

69. Liu, Z., J. Shi, and Y. Wang. *Evaluating Tensile Properties of 3D Printed Continuous Fiber Reinforced Nylon 6 Nanocomposites*. in *International Manufacturing Science and Engineering Conference*. 2018. American Society of Mechanical Engineers.

70. Liu, S., Y. Li, and N. Li, *A novel free-hanging 3D printing method for continuous carbon fiber reinforced thermoplastic lattice truss core structures.* Materials & Design, 2018. **137**: p. 235-244.

71. Liu, T., et al., *Interfacial performance and fracture patterns of 3D printed continuous carbon fiber with sizing reinforced PA6 composites.* Composites Part A: Applied Science and Manufacturing, 2018. **114**: p. 368-376.

72. Luan, C., et al., *Large-scale deformation and damage detection of 3D printed continuous carbon fiber reinforced polymer-matrix composite structures.* Composite Structures, 2019. **212**: p. 552-560.

73. Luo, H., et al., *Selectively enhanced 3D printing process and performance analysis of continuous carbon fiber composite material.* Materials, 2019. **12**(21): p. 3529.

74. Matsuzaki, R., et al., *Three-dimensional printing of continuous-fiber composites by in-nozzle impregnation.* Scientific reports, 2016. **6**(1): p. 1-7.

75. Mei, H., et al., *Tailoring strength and modulus by 3D printing different continuous fibers and filled structures into composites.* Advanced Composites and Hybrid Materials, 2019. **2**(2): p. 312-319.

76. Melenka, G.W., et al., *Evaluation and prediction of the tensile properties of continuous fiber-reinforced 3D printed structures.* Composite Structures, 2016. **153**: p. 866-875.

77. Ming, Y., et al., *Fabrication of continuous glass fiber-reinforced dual-cure epoxy composites via UV-assisted fused deposition modeling.* Composites Communications, 2020. **21**: p. 100401.

78. Ming, Y., et al., *Investigation on process parameters of 3D printed continuous carbon fiber-reinforced thermosetting epoxy composites.* Additive Manufacturing, 2020. **33**: p. 101184.

79. Mohammadizadeh, M., et al., *Creep behavior analysis of additively manufactured fiber-reinforced components.* The International Journal of Advanced Manufacturing Technology, 2018. **99**(5): p. 1225-1234.

80. Mohammadizadeh, M., et al., *3D printed fiber reinforced polymer composites-Structural analysis.* Composites Part B: Engineering, 2019. **175**: p. 107112.

81. Mori, K.-i., T. Maeno, and Y. Nakagawa, *Dieless forming of carbon fibre reinforced plastic parts using 3D printer.* Procedia engineering, 2014. **81**: p. 1595-1600.

82. Mosleh, N., A.M. Rezadoust, and S. Dariushi, *Determining process-window for manufacturing of continuous carbon fiber-reinforced composite Using 3D-printing.* Materials and Manufacturing Processes, 2021. **36**(4): p. 409-418.

83. Nabipour, M. and B. Akhoundi, *An experimental study of FDM parameters effects on tensile strength, density, and production time of ABS/Cu composites.* Journal of Elastomers & Plastics, 2020: p. 0095244320916838.

84. Naranjo-Lozada, J., et al., *Tensile properties and failure behavior of chopped and continuous carbon fiber composites produced by additive manufacturing.* Additive Manufacturing, 2019. **26**: p. 227-241.

85. O'Connor, H.J. and D.P. Dowling, *Low-pressure additive manufacturing of continuous fiber-reinforced polymer composites.* Polymer Composites, 2019. **40**(11): p. 4329-4339.

86. Oztan, C., et al., *Microstructure and mechanical properties of three dimensional-printed continuous fiber composites.* Journal of Composite Materials, 2019. **53**(2): p. 271-280.

87. Peng, Y., et al., *Tailorable rigidity and energy-absorption capability of 3D printed continuous carbon fiber reinforced polyamide composites.* Composites Science and Technology, 2020. **199**: p. 108337.

88. Prajapati, A.R., H.K. Dave, and H.K. Raval, *An Experimental Study on Mechanical, Thermal and Flame-Retardant Properties of 3D-Printed Glass-Fiber-Reinforced Polymer Composites.* Journal of Materials Engineering and Performance, 2021: p. 1-12.

89. Prajapati, A.R., H.K. Dave, and H.K. Raval, *Effect of fiber volume fraction on the impact strength of fiber reinforced polymer composites made by FDM process.* Materials Today: Proceedings, 2021.

90. Prajapati, A.R., H.K. Dave, and H.K. Raval, *Effect of fiber reinforcement on the open hole tensile strength of 3D printed composites.* Materials Today: Proceedings, 2021.

91. Pyl, L., K.-A. Kalteremidou, and D. Van Hemelrijck, *Exploration of specimen geometry and tab configuration for tensile testing exploiting the potential of 3D printing freeform shape*

continuous carbon fibre-reinforced nylon matrix composites. Polymer Testing, 2018. **71**: p. 318-328.

92. Qiao, J., Y. Li, and L. Li, *Ultrasound-assisted 3D printing of continuous fiber-reinforced thermoplastic (FRTP) composites.* Additive Manufacturing, 2019. **30**: p. 100926.

93. Quan, C., et al., *3D printed continuous fiber reinforced composite auxetic honeycomb structures.* Composites Part B: Engineering, 2020. **187**: p. 107858.

94. Sanei, S.H., A. Arndt, and R. Doles, *Open hole tensile testing of 3D printed continuous carbon fiber reinforced composites.* Journal of Composite Materials, 2020. **54**(20): p. 2687-2695.

95. Sanei, S.H.R., et al. *Mechanical Properties of 3D Printed Fiber Reinforced Thermoplastic*. in *ASME 2019 International Mechanical Engineering Congress and Exposition*. American Society of Mechanical Engineers Digital Collection.

96. N. Sarvestani, A., et al. *3D printed composites with continuous carbon fiber reinforcements*. in *ASME International Mechanical Engineering Congress and Exposition*. 2017. American Society of Mechanical Engineers.

97. Shi, K., et al., *3D printing Kevlar fiber layer distributions and fiber orientations into nylon composites to achieve designable mechanical strength.* Additive Manufacturing, 2021. **39**: p. 101882.

98. Shiratori, H., et al., *Compressive strength degradation of the curved sections of 3D-printed continuous carbon fiber composite.* Composites Part A: Applied Science and Manufacturing, 2021. **142**: p. 106244.

99. Sugiyama, K., et al., *3D printing of optimized composites with variable fiber volume fraction and stiffness using continuous fiber.* Composites Science and Technology, 2020. **186**: p. 107905.

100. Sugiyama, K., et al., *3D printing of composite sandwich structures using continuous carbon fiber and fiber tension.* Composites Part A: Applied Science and Manufacturing, 2018. **113**: p. 114-121.

101. Tian, X., et al., *Recycling and remanufacturing of 3D printed continuous carbon fiber reinforced PLA composites.* Journal of cleaner production, 2017. **142**: p. 1609-1618.

102. Tian, X., et al., *Interface and performance of 3D printed continuous carbon fiber reinforced PLA composites.* Composites Part A: Applied Science and Manufacturing, 2016. **88**: p. 198-205.

103. Todoroki, A., et al., *Tensile property evaluations of 3D printed continuous carbon fiber reinforced thermoplastic composites.* Advanced Composite Materials, 2020. **29**(2): p. 147-162.

104. Touchard, F., et al., *Interfacial adhesion quality in 3D printed continuous CF/PA6 composites at filament/matrix and interlaminar scales.* Composites Part B: Engineering, 2021: p. 108891.

105. Van Der Klift, F., et al., *3D printing of continuous carbon fibre reinforced thermo-plastic (CFRTP) tensile test specimens.* Open Journal of Composite Materials, 2016. **6**(01): p. 18.

106. Vaneker, T., *Material extrusion of continuous fiber reinforced plastics using commingled yarn.* Procedia CIRP, 2017. **66**: p. 317-322.

107. Wang, K., et al., *Simultaneous reinforcement of both rigidity and energy absorption of polyamide-based composites with hybrid continuous fibers by 3D printing.* Composite Structures, 2021. **267**: p. 113854.

108. Wang, X., et al., *3D Printing of Continuous Fiber Reinforced Low Melting Point Alloy Matrix Composites: Mechanical Properties and Microstructures.* Materials, 2020. **13**(16): p. 3463.

109. Wang, Y., et al., *Process parameters and mechanical properties of continuous glass fiber reinforced composites-polylactic acid by fused deposition modeling.* Journal of Reinforced Plastics and Composites, 2021: p. 0731684421998017.

110. Yang, C., et al., *3D printing for continuous fiber reinforced thermoplastic composites: mechanism and performance.* Rapid Prototyping Journal, 2017.

111. Yao, X., et al., *Evaluation of carbon fiber-embedded 3D printed structures for strengthening and structural-health monitoring.* Materials & Design, 2017. **114**: p. 424-432.

112. Yin, L., et al., *Characterizations of continuous carbon fiber-reinforced composites for electromagnetic interference shielding fabricated by 3D printing.* Applied Physics A, 2019. **125**(4): p. 1-11.

113. Yu, T., et al., *Tensile and flexural behaviors of additively manufactured continuous carbon fiber-reinforced polymer composites.* Composite Structures, 2019. **225**: p. 111147.

114. Zeng, C., et al., *Bending performance and failure behavior of 3D printed continuous fiber reinforced composite corrugated sandwich structures with shape memory capability.* Composite Structures, 2021. **262**: p. 113626.

115. Zhang, J., et al., *Performance of 3D-printed continuous-carbon-fiber-reinforced plastics with pressure.* Materials, 2020. **13**(2): p. 471.

116. Zhang, Y., et al., *Prediction of deformation and failure behavior of continuous fiber reinforced composite fabricated by additive manufacturing.* Composite Structures, 2021. **265**: p. 113738.

117. Chacón, J., et al., *Additive manufacturing of PLA structures using fused deposition modelling: Effect of process parameters on mechanical properties and their optimal selection.* Materials & Design, 2017. **124**: p. 143-157.